SOME THERMODYNAMIC PROPERTIES OF RARE EARTH THIOFLUORIDE AND Caβ″-ALUMINA COMPOUNDS

SOME THERMODYNAMIC PROPERTIES OF RARE EARTH THIOFLUORIDE AND Caβ″-ALUMINA COMPOUNDS

By

MARK KOCH, B.Eng.

A Thesis

Submitted to the School of Graduate Studies

in Partial Fulfilment of the Requirements

for the Degree

Master of Engineering

McMaster University

April 1988

MASTER OF ENGINEERING (April 1988)
(Materials Science and Engineering)

McMASTER UNIVERSITY
Hamilton, Ontario

TITLE: SOME THERMODYNAMIC PROPERTIES OF RARE EARTH THIOFLUORIDE AND Caβ″-ALUMINA COMPOUNDS

AUTHOR: Mark Koch, B.Eng. (University)

SUPERVISOR: Dr. D.A.R. Kay

NUMBER OF PAGES: xii, 82.

ABSTRACT

Thermodynamic measurements were taken using calcia stabilized zirconia and Caβ"-alumina solid electrolytes in reversible galvanic cells.

The high temperature thermodynamic properties of eight rare earth thiofluorides were studied by preparing them in the laboratory and constructing the following type of galvanic cell:

$$Pt/Ag(s), Ag_2S(s), ReSF(s), ReOF(s)/CSZ/Air/Pt$$

The standard free energies of formation of the corresponding rare earth thiofluorides, were calculated from e.m.f. measurements, and found found to be:

Compound	Standard Free Energy of Formation $\Delta G^\circ = A + BT(K)$ [cal]		Error ±cal	Temp. Range (K)
	"A"	"B"		
LaSF	−256120	44.52	2884	919-1088
CeSF	−247722	38.65	3235	925-1086
PrSF	−254615	47.13	5261	931-1083
SmSF	−246674	42.04	2811	923-1084
TbSF	−242082	37.26	3773	933-1085
HoSF	−239807	25.02	2870	939-1087
YbSF	−244316	47.57	3457	913-1090
YSF	−244088	37.75	3515	925-1087

Values in calories may be converted to joules by multiplying by 4.182.

The desulphurising capability of the rare earth oxyfluorides was investigated since these compounds are found in the calcined bastnaesite ores, used in gaseous desulphurisation. The desulphurising potentials of the oxyfluorides were determined by considering the reaction

$$ReOF(s) + \frac{1}{2}S_2(g) \rightarrow ReSF(s) + \frac{1}{2}O_2(g)$$

and it was found that the rare earth oxides have a greater desulphurising potential than the rare earth oxyfluorides.

The periodic trend exhibited by the results of this investigation were plotted with the values obtained by other investigations of the rare earth mono-sulphides, rare earth oxyfluorides and the rare earth sesquioxides. A good correlation is observed between the trends exhibited by these various compounds of the lanthanide series.

Three compositions of Caβ''-alumina solid electrolyte (see table below) reported in Kumar's[16] work, were made in the laboratory for use in galvanic cells. Thermodynamic measurements made using these Caβ''-alumina solid electrolytes were used to determine the stabilities of these electrolytes and to assess the potential use of this family of solid electrolyte as a high temperature oxygen and.or calcium probe.

COMPOSITION	CaO	MgO	Al_2O_3	PHASES
(a)	1.0	0.6	6.0	β''
(b)	1.0	0.8	8.0	β'', $MgO.Al_2O_3$ α-Al_2O_3
(c)	1.0	1.2	6.0	β'', $MgO.Al_2O_3$ $CaO.2Al_2O_3$

The chemical stability of these electrolytes was assessed by constructing the following types of galvanic cell:

$$Pt/Ni(s), NiO(s)/Ca\beta''\text{-alumina(b)}/Ni(s), NiF_2(s), CaF_2(s)/Pt$$

$$Pt/CeO_2(s), CeF_3(s), CaO(\beta''\text{-alumina(a)}, CaF_2/CSZ/Air/Pt$$

The activity of CaO was determined for the three electrolyte compositions from the measured cell emf's:

$$\ell n\, aCaO(\beta'',b) = 1.17 - 25169/T - 3.87 \log T$$

$$T(K) = 900 - 1100$$

$$\ell n\, aCaO(\beta'',c) = 6.51 - 25750/T - 3.87 \log T$$

$$T(K) = 900 - 1100$$

$$\ell n\, aCaO(\beta'', a) = 7.05 - 26{,}864/T$$

$$T(K) = 950 - 1333$$

The stabilities of these electrolytes at high temperatures and low oxygen potentials, like those found in liquid iron or steel, were also established. It was found that these electrolytes are stable under these conditions.

ACKNOWLEDGEMENTS

I wish to thank Dr. D.A.R. Kay for his support, guidance and suggestions given during the course of this study.

Thanks are also due to K. Bala-Subramanian for his interest and the many valuable discussions we had together.

I would especially like to acknowledge D. Misale for her work in preparing many diagrams in this thesis and the Engineering Word Processing Centre who prepared the text.

The author also gratefully acknowledges the Department of Materials Science and Engineering, fellow graduate students and the technical staff of the Department for their help.

TABLE OF CONTENTS

TABLE OF CONTENTS (continued)

TABLE OF CONTENTS (continued)

LIST OF ILLUSTRATIONS

LIST OF ILLUSTRATIONS

LIST OF TABLES

CHAPTER 1

INTRODUCTION AND BACKGROUND

1.1 Introduction

This investigation is concerned with the characterisation and use of solid electrolytes to measure the thermodynamic properties of oxide and sulphide compounds. The potential use of these electrolytes as calcium and oxygen sensing devices with particular application to measurements in molten iron and steel, is also investigated.

1.2 Present Study

More specifically, this investigation can be broken into two distinct parts:

1) Using calcia stabilized zirconia (CSZ) solid electrolytes, the thermodynamic properties of eight rare earth thiofluorides were measured to determine their potential desulphurisation capacity in the conversion of rare earth oxyfluoride to rare earth thiofluoride.

2) Three compositions of Caβ''-alumina solid electrolyte were synthesized from elemental oxide powders in order to characterise and establish the basis for the potential use of these electrolytes as calcium and oxygen sensors. The processing and manufacturing of Caβ''-alumina pellets was an integral part of this investigation.

1.3 Rare Earth Derivatives of Bastnaesite Concentrates

1.3.1 Introduction

Rare earth oxyfluorides are a major constituent in calcined bastnaesite ore concentrates found in the Mountain Pass region of California. This thermodynamic investigation of the conversion of rare earth oxyfluoride to rare earth thiofluoride was undertaken in order to establish the desulphurisation capacity of this lanthanide series of compounds. Uncalcined bastnaesite concentrates from the Mountain Pass ore bodies of California are essentially rare earth hydroxyfluorocarbonates which, when calcined, are converted to mainly cerium dioxide and rare earth oxyfluorides. A typical composition of these concentrates is given in Appendix I (1). These calcined bastnaesite concentrates are intermediate products which are further refined to eventually produce the rare earth metals.

1.3.2 The Rare Earth Oxyfluoride and Thiofluoride Compounds

The crystallographic nature of the rare earth oxyfluorides was first investigated by W.H. Zachariasen (2), Finkelnberg and Stein (3), and by Baenziger et al. (4), who determined that the lanthanide series of rare earth oxyfluorides had a rhombohedral structure except cerium oxyfluoride which was cubic face centred.

The thermodynamic properties of these rare earth oxyfluorides were recently investigated by Hong, Kumar and Kay (5), (6), who determined the thermodynamics of Re-O-F compounds (Re = La,Ce,Pr,Nd,Sm,Tb,Dy,Ho,Er,Yb,Y) in the temperature range 925 to 1125 K. In their investigation, the standard free energies of formation of the rare earth oxyfluorides were determined from the EMFs of reversible galvanic cells using CSZ (calcia stabilized zirconia) and Caβ"-alumina solid electrolytes.

The only information which is available in the literature on the rare earth thiofluorides is work which was carried out by Schmid and Hahn (7) in their investigation of

LaSF, CeSF and EuSF. These rare earth compounds were produced by heating intimate mixtures of the rare earth fluoride and corresponding rare earth sulphide in evacuated quartz capsules. They found that these rare earth thiofluoride compounds crystallize with the PbFCl (matlockite), tetragonal crystal structure (46), and published the powder X-ray diffraction patterns which, to the author's knowledge, are the only available diffraction patterns in this lanthanide series of rare earth thiofluoride compounds. One would strongly suspect that these compounds would be isostructural, as other lanthanide series of compounds have exhibited this trend (2), (4).

Verkhovets et al. (8), determined the phase diagrams of the lanthanum sulfide/-lanthanum oxide and the lanthanum sulphide/lanthanum fluoride systems. They confirmed the existence and stability of the lanthanum thiofluoride phase which was found to be stoichiometric with a melting point of 2093 K. There is no thermodynamic data available for the lanthanide series of rare earth thiofluoride compounds.

1.4 Caβ''-alumina Solid Electrolyte

Choudhury (9) was one of the first investigators to make thermodynamic measurements with the Naβ-alumina electrolyte. In his investigations, he used two phase alpha and beta alumina compositions to measure the soda activity in his electrolyte material using the following cell:

$$\text{Pt/Ni, NiF, NaF/alpha + beta alumina/Cu, } Cu_2O\text{/Pt} \qquad (1.1)$$

and he also successfully measured oxygen potentials established by metal-metal oxide electrodes using the cell:

$$\text{Pt/Ni, NiO/alpha + beta alumina/Cu, } Cu_2\,O\text{/Pt} \qquad (1.2)$$

According to the phase rule, a two phase, three component system such as Naβ-alumina has only one degree of freedom at a given temperature and pressure. In cell 1.2, the

two electrodes establish the oxygen chemical potential, which fixes the relationship of the chemical potentials of Na, Al and O at the electrode/electrolyte interface. This relationship can be determined by solving the Gibbs-Duhem equation for the α-alumina and β-alumina phases giving the following results:

$$d\mu_{Al} = 3d\mu_{Na} \tag{1.3}$$

$$d\mu_{O} = -2d\mu_{Na} \tag{1.4}$$

Substituting these equations into the Wagner relationships (1.5) and (1.6), which describe the emf of a reversible galvanic cell, we obtain equations (1.7) and (1.8).

$$E = \frac{1}{F}\int_{C}^{A} d\mu_{Na} \tag{1.5}$$

where: F = faraday constant

A = anode

C = Cathode

E = emf

This equation on integration yields:

$$E = \frac{RT}{F}\,\ell n\left(a^{A}_{Na}/a^{C}_{Na}\right) \tag{1.6}$$

Substituting equations (1.3) and (1.4) into (1.5), we obtain:

$$E = \frac{1}{3F}\int_{C}^{A} d\mu_{Al} \tag{1.7}$$

$$E = -\frac{1}{2F}\int_{C}^{A} d\mu_{O} \tag{1.8}$$

Integrating these equations yields:

$$E = \frac{RT}{F}\,\ell n\,\frac{a^{A}_{Na}}{a^{C}_{Na}} = \frac{RT}{3F}\,\ell n\,\frac{a^{A}_{Al}}{a^{C}_{Al}} = \frac{RT}{2F}\,\ell n\,\frac{a^{A}_{O}}{a^{C}_{O}} \tag{1.9}$$

One can see that two phase Naβ-alumina can be used to measure oxygen potentials, and similarly, in principle, the three phase, four component form of Caβ"-alumina can also be used to measure oxygen potentials.

Elrefaie (10) was also able to use the two phase (alpha-beta), Naβ-alumina solid electrolyte to measure soda activities in his material and oxygen potentials as low as those established by Al-Al_2O_3 coexistences. From this work Choudhury (30) and Elrefaie (10) concluded that two phase Naβ-alumina could be used to measure extremely low oxygen partial pressures which are outside the electrolytic domain of oxide anion conducting electrolytes.

The work on Naβ-alumina electrolyte, in which Na ions have been exchanged in molten salts by Ag, K, Rb, Li, NH, Ca, Cu, La, and Ga (11), (12), (13), (14), (15), has led researchers to investigate the possibility of synthesizing other β-aluminas with the intent of making a wide variety of electrolytes with different conducting species available for thermodynamic investigations using galvanic cells.

Kumar (16) was successful in synthesizing Laβ-alumina, Kβ-alumina, Caβ-alumina and Caβ''-alumina. The potential use of Caβ''-alumina as a calcium and oxygen sensor in high temperature environments is of particular interest and has led to this investigation into the manufacturing, processing and characterisation of the Caβ''-alumina family of solid electrolytes.

CHAPTER 2

CSZ AND β-ALUMINA SOLID ELECTROLYTES FOR THE MEASUREMENT OF HIGH TEMPERATURE THERMODYNAMIC PROPERTIES

2.1 Introduction

A solid electrolyte is a material in which, as in liquid electrolytes, electrical conduction occurs predominantly by the transport of charged ions. It is the near absence of any electronic contribution to the total conductivity in these materials that render them useful in the construction of reversible galvanic cells for the measurement of high temperature thermodynamic properties.

The initial work carried out by Kiukkola and Wagner (17) on oxide solid electrolytes in 1957, laid the foundation for the development of the zirconia and thoria based oxygen conducting solid electrolytes which have since been extensively used to measure the thermodynamic properties of a wide variety of materials.

Similarly, the work by Yao and Kummer (11) led to the emergence of the family of β-alumina solid electrolytes which are becoming an increasingly important electrolyte in the measurement of thermodynamic properties. In this section, a brief review of the properties and applications of these electrolytes is given.

2.2 Oxygen Conducting Solid Electrolytes

The oxygen ion conducting solid electrolyte is one of the most commonly used electrolytes for high temperature thermodynamic measurements, electrochemical probes and high temperature fuel cells. These electrolytes are solid solutions of lime doped zirconia or yittria doped thoria. The addition of the dopent has a two fold effect. Zirconia, for example, has a

monoclinic crystal structure from room temperature to 1473 K and a tetragonal structure from 1473 to 2573 K. Firstly, the addition of calcium oxide to zirconia stabilizes the high temperature fluorite crystal structure which is a face centered cubic arrangement of metal cations with the oxygen anions occupying the tetrahedrally coordinated sites as shown in Figure (2.1). Secondly, the aliovalent dopant introduces defects in the lattice (i.e. the addition of one calcium ion creates one oxygen vacancy on the oxygen sublattice), which significantly increases the ionic conductivity of the oxide, since it is essentially the ionic defects present in the oxides which give rise to the ionic conductivity. A summary of the defect equilibria and their effect is given below.

2.2.1 Defects and their Influence Upon Conductivity and the Electrolytic Domain

It is the presence of ionic defects which gives rise to ionic conduction. At any given temperature there is a finite concentration of intrinsic ionic defects in a solid as a result of the entropy contribution to the Gibbs free energy. The most common ionic defects encountered are vacancy pairs which are known as Schottky defects or vacancy-interstitial pairs which are known as Frenkel defects. Electronic defects on the other hand are a result of thermal excitation of electrons "n" from the valence band to the conduction band, and the presence of holes "p" in the valence band. This can be expressed mathematically as follows;

$$[n][p] \propto \mathrm{Exp}[-Eq/kT] \qquad Eq = \text{Band Gap Energy} \tag{2.1}$$

$$\begin{aligned} \sigma_{TOT} &= \sigma_{ionic} + \sigma_n + \sigma_p \\ &= \sum [c] q^2 \mu_i + [n] q^2 \mu_n + [p] q^2 \mu_p \end{aligned} \tag{2.2}$$

where:

μ = mobility

q = electrical charge

σ = electrical conductivity

[ ] = represent concentrations

c = ionic defects.

Physical measurements have shown that mobilities of electronic defects in ionic solids are of the order 100 to 1000 times greater than the mobility of ionic defects (18). Therefore ionic conduction can only dominate for materials which have a relatively large band gap (of the order >3eV).

The predominant intrinsic ionic defects in zirconia are oxygen vacancies (V_o) and oxygen interstitials (O_i). Using the Kroger Vink notation, where the symbol indicates the defect, the subscript the location, the superscript the effective charge, and brackets represent concentrations, we can write defect equilibria, noting that charge neutrality must be maintained.

$$O_o = O_i^{=} + V_o^{++} \tag{2.3}$$

$$[p] + 2[V_o^{++}] = [n] + 2[O_i^{=}] \tag{2.4}$$

The oxygen pressure will disturb this equilibria and with the presence of high oxygen pressures the extrinsic defect equilibria will be:

$$\frac{1}{2} O_2 = O_i^{=} + 2p^{+} \quad \text{when } K = \frac{[O_i^{=}][p]^2}{P_{O_2}^{1/2}} \tag{2.5}$$

$$[p] \propto P_{O_2}^{1/4} \qquad \text{for } [O_i^{=}] \text{ very large and essentially constant} \tag{2.6}$$

and for low oxygen pressures we have:

$$O_o = \frac{1}{2} O_2 + V_o^{++} + 2n^{-} \quad \text{where } K = \frac{[V_o^{++}] P_{O_2}^{1/2} [n]^2}{[O_o]} \tag{2.7}$$

$$[n] \propto P_{O_2}^{-1/4} \qquad \text{for } [O_o] \approx 1, V_o^{++} \text{ very large and essentially constant} \tag{2.8}$$

We see that at high and low oxygen partial pressures the conductivity of the electrolyte will vary with oxygen pressure while at some intermediate oxygen pressures the concentration of defects will be intrinsically determined and hence the conductivity will be independent of oxygen partial pressure as illustrated in Figure 2.2A.

In Figure 2.2, we see that there is a regime of oxygen pressure over which ionic conduction is predominant and that adding an aliovalent dopent enlarges this regime which is known as the "electrolytic domain". Figure 2.2B is a schematic plot of the concentration of ionic and electronic defects for the hypothetical compound Mx_2 as a function of Px_2. This plot is derived from considering defect equilibria analogous to those above in equations (2.5) to (2.8). The plot shows that electron conduction is predominant at low oxygen partial pressures, hole conduction is predominant at high oxygen partial pressures, and that ionic conduction is predominant at intermediate oxygen partial pressures which is the electrolytic domain. Conduction in this region is independent of the oxygen partial pressure as indicated in Figure 2.2A.

The size of the electrolytic domain is also dependent upon temperature as well as oxygen pressure and defines the operating regime in which the electrolyte can be successfully used in a reversible galvanic cell. Diagram 2.2C depicts the electrolytic domain as a function of temperature and oxygen partial pressure. The boundaries shown are drawn for electronic conductivities which contribute less than or equal to 1% of the total conductivity. Within the electrolytic domain conductivities have been measured at 1273 K and are of the order 0.05 ohms per cm for a zirconia 13 mole % lime doped solid electrolyte.

2.3 The β-alumina Solid Electrolyte

The β-aluminas are a family of solid electrolytes which can be made with a variety of different conducting ionic species including Sr, Pb, Ba, Sn, Mn, Ca, Cu, Ga, K, Na, (11), (12),

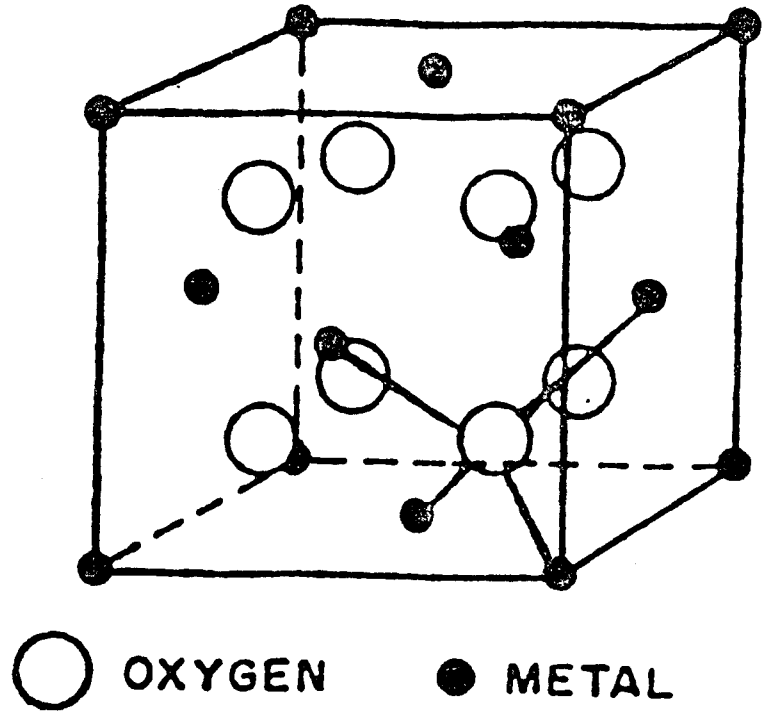

Figure 2.1: The fluorite crystal structure.

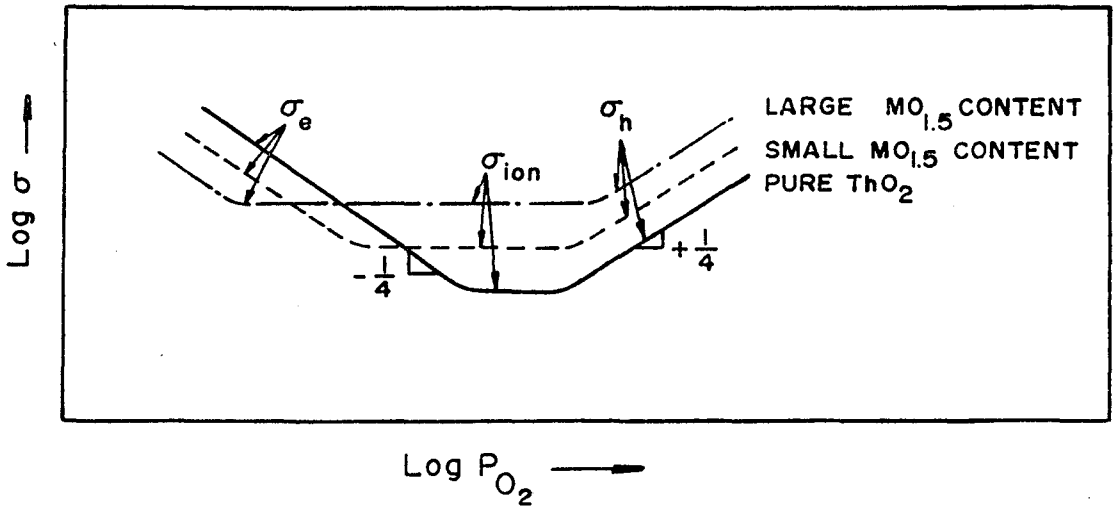

Figure 2.2A: Schematic representation of the electrical conductivity for the compound MO_2.

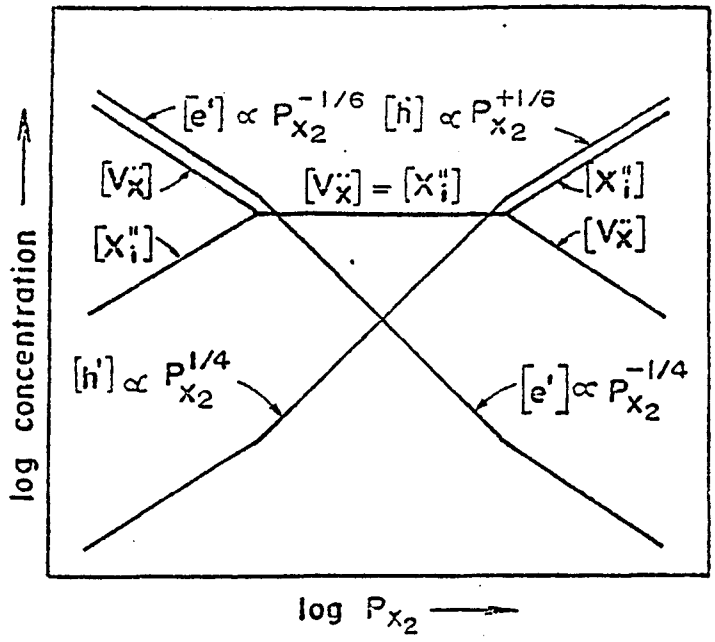

Figure 2.2B: Schematic representation of concentration of ionic and electronic defects as a function of P_{X_2} (symbols defined in text).

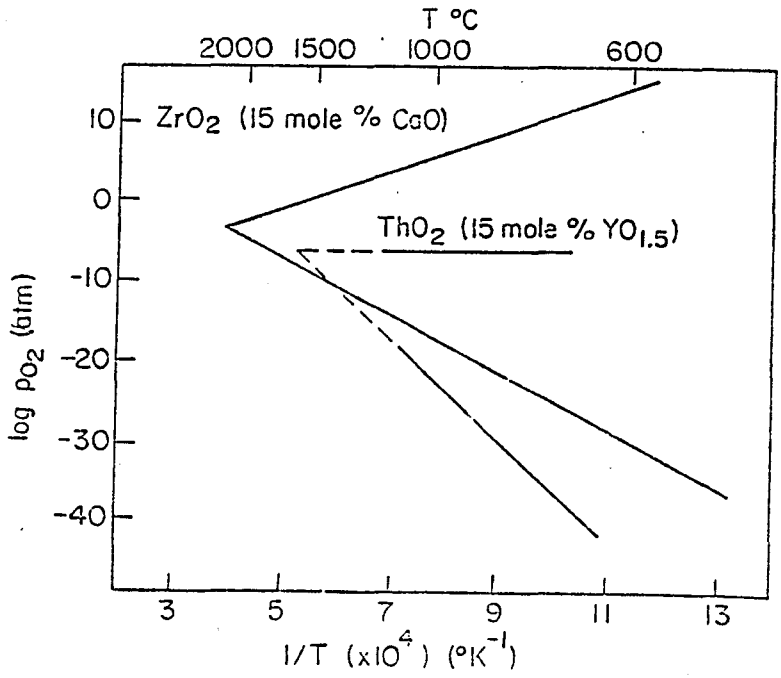

Figure 2.2C: Electrolytic domains of ZrO_2 (+CaO) and ThO_2 (+Y_2O_3).

(19). Of these, Naβ-alumina has stimulated the most interest in the β-aluminas because of its ease of manufacture and its application in high energy density sodium-sulphide batteries. The β-aluminas have excellent solid electrolyte properties:

1) High ionic conductivity.

2) Good mechanical strength.

3) Stability and lack of reactivity in corrosive and high temperature environments.

2.3.1 Composition and Crystal Structure

The β-aluminas have the general formula $M_xO_y \cdot nAl_2O_3$ and range in composition from n= 5-11 for x= 1,2 and y= 1,3. The phase diagram for the soda-alumina system is still uncertain, however the proposed diagrams of Devries and Roth (20) and Weber and Venero (21) are depicted in Figures (2.3) and (2.4). Devries and Roth found that two β-alumina like phases exist in the composition ranges soda:alumina = 1:9 to 1:11 and 1:5 to 1:7. These two common forms of this material are referred to as β-alumina which has the hexagonal crystal structure and β"-alumina which has the rhombohedral form, respectively.

Naβ-alumina has the stoichiometric formula $Na_2O\text{-}11Al_2O_3$, but in practice, it usually contains excess soda. Naβ"-alumina, which has the stoichiometric formula $Na_2O\text{-}5Al_2O_3$, is soda deficient and usually contains magnesia or lithia to stabilize the high temperature crystal structure.

The crystal structure of Naβ-alumina as determined by Beevers and Ross (22) shows that the Al(3+) and O(2−) ions are packed in the same fashion as in the $MgAl_2O_4$ spinel, with the difference that the Al(3+) ions occupy both octahedral and tetrahedral sites. The $MgAl_2O_4$ like "spinel blocks" are separated by loosely packed planes which contain Na(1+) and O(2−) ions. This is known as the conduction plane. (See Figures 2.5A and 2.5B.)

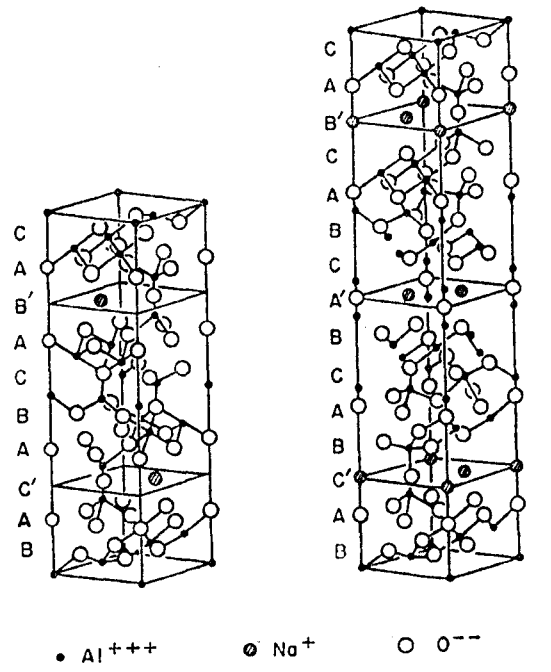

Figure 2.3A: Structure of β-alumina (left) and β″-alumina (right). The Na atoms in β-alumina are shown in Beevers-Ross (BR) sites (38).

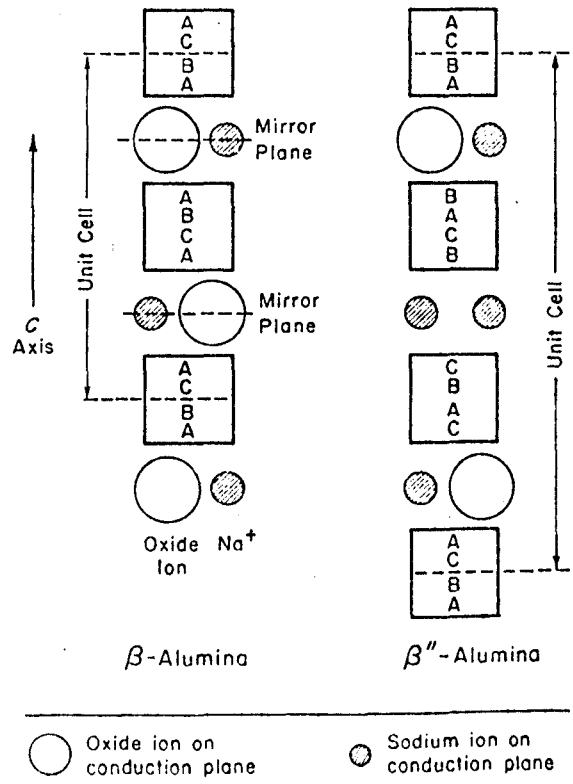

Figure 2.3B: Oxide ion packing arrangements in β-alumina and β″-alumina. (Note: letters refer to stacking arrangement where ABC represents face-centered cubic packing while ABAB would represent hexagonal packing (38).)

(a)

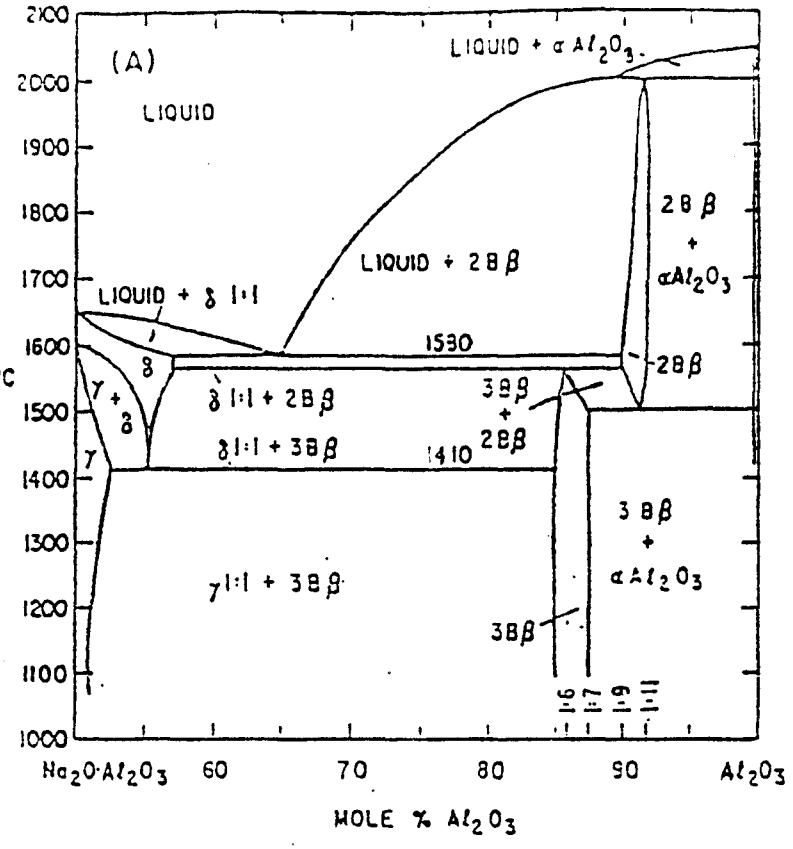

(b)

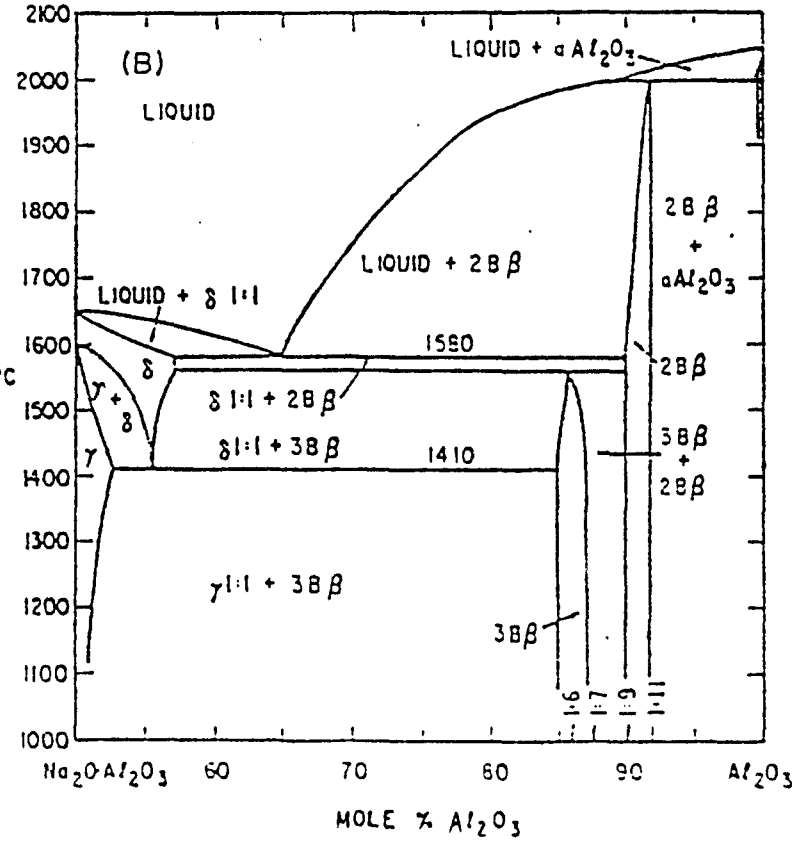

Figure 2.4: Equilibrium diagram for the system $NaAlO_2$–Al_2O_3 as proposed by DeVries and Roth (20).

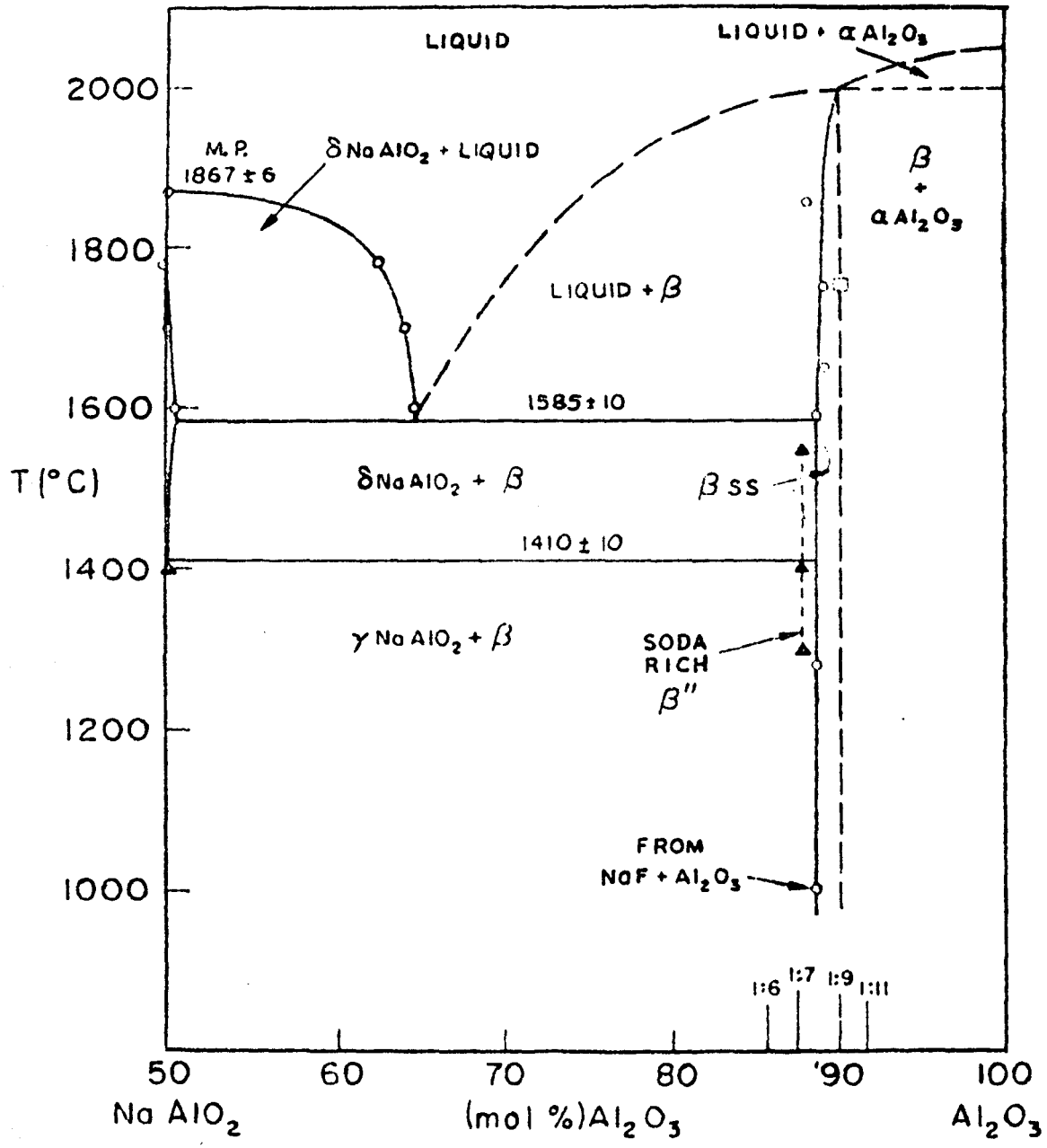

Figure 2.5: Equilibrium diagram for the system $NaAlO_2$–Al_2O_3 as proposed by Weber and Venero (21).

The spinel block itself is cubic, however the additional conduction planes lead to an hexagonal form (for β-alumina) which consists of two spinel blocks in which the conduction plane is a mirror plane for the blocks. In β"-alumina the conduction plane is not a mirror plane, but rather the stacking arrangement of the spinel blocks is repeated for every three spinel blocks. this results in a rhombohedral form with an a-axis of about 5.6 angstroms and c-axis of 33.5 angstroms as compared to 5.6 and 22.5 angstroms respectively for β-alumina (15).

The movement of $Na(1+)$ ions, which gives rise to ionic conduction, is limited to the loosely packed conduction planes and is extremely difficult in the c-direction, resulting in the anisotropic nature of the conduction path. The ionic conductivity of β"-alumina ($0.63\,(\Omega\,cm)^{-1}$ at 1000 K) has been reported to be higher than β-alumina ($0.25\,(\Omega\,cm)^{-1}$ at 1000 K). This is thought to be a result of a larger number of available charge carriers in the conduction planes and the somewhat higher mobility of the conducting species (23).

CHAPTER 3

THERMODYNAMIC INVESTIGATIONS USING GALVANIC CELLS WITH SOLID ELECTROLYTES

3.1 The Thermodynamic Treatment of EMF Measurements and Their Uncertainties

Results from the use of reversible galvanic cells to generate EMF data are used in the calculation of: a) the Gibbs free energy change for the virtual cell reaction b) the activity or partial pressures of various components and c) the enthalpy and entropy changes of the virtual cell reaction from the temperature dependence of the cell EMF.

In practice, in order to avoid any polarization effects, the reversible potential difference is measured at open circuit with a high impedance voltmeter. The EMF is taken as positive by the Stockholm convention if the right-hand electrode of the galvanic cell is positive. Using this convention the cell EMF multiplied by nF (where n the charge transfer, is chosen to correspond to one formula conversion and F is the Faraday constant), gives the maximum electrical work obtained, which is equal to the negative Gibbs free energy change of the virtual cell reaction.

$$\Delta G = -nFE \tag{3.1}$$

It is important that the cell EMFs used in the above equation are those measured reversibly; in other words under conditions in which no energy is being introduced or extracted from the cell. This treatment is not valid when there is a net current flow and a reaction proceeds irreversibly.

From the temperature dependance of the EMFs one can calculate the enthalpy and entropy changes of the virtual cell reaction. The Gibbs free energy change, considering

extensive properties in a reaction, is given by:

$$d\Delta G = \Delta V dP - \Delta S dT \tag{3.2}$$

or at constant pressure:

$$\left(\frac{\partial \Delta G}{\partial T}\right)_p = -\Delta S \tag{3.3}$$

This is the well known Gibbs Helmholtz equation. Now differentiating equation (3.1), with respect to temperature yields:

$$\left(\frac{\partial \Delta G}{\partial T}\right)_p = -nF\left(\frac{\partial E}{\partial T}\right)_p \tag{3.4}$$

Combining equations (3.3) and (3.4):

$$\Delta S = nF\left(\frac{\partial E}{\partial T}\right)_p \tag{3.5}$$

Similarly if we substitute equations (3.5) and (3.1) into (3.2) we have:

$$\Delta H = -nF\left[E - T\left(\frac{\partial E}{\partial T}\right)_p\right] \tag{3.6}$$

3.1.1 Experimental Errors

The experimental uncertainty in EMF measurements in open circuit reversible galvanic cells is considered to be ± 1 mv which for an oxygen concentration cell for example corresponds to ± 46 cal. per gm. atom of oxygen in the Gibbs free energy change. Schmalzreid (24) considers that the uncertainty in ΔH is usually about ± 500 cal. per gm atom due to the relatively narrow temperature range over which the EMF measurements are taken. Wagner (17) noted that high temperature enthalpy values obtained from electrochemical cell measurements may in some cases be more accurate than calorimetric measurements.

3.2 Practical Design and Limitations

A galvanic cell consists of two electrodes in intimate contact with a solid electrolyte which is usually in the form of a disk shaped pellet or closed end tube. The successful opera-

tion of the galvanic cell requires that firstly, the components in the electrode compartments coexist under the experimental conditions and that chemical equilibrium is established at the electrode-electrolyte interface. Secondly, there should be no reaction between the electrodes and the electrolyte which could alter the electrolyte and thirdly, the measured potentials should lie within the electrolytic domain of the electrolyte used. Patterson et al. (25) reported that calcia stabilized zirconia can be used for thermodynamic measurements at 1273 K over the oxygen partial pressure range 10 EXP-23 to 10 EXP5 atm. β-alumina solid electrolytes have been used by Elrefaie (10) and Choudhury (9) to measure oxygen partial pressures as low as that established by the Al-Al_2O_3 coexistance.

3.2.1 Galvanic Cell Designs and Experimental Considerations

Galvanic cell designs can be broken into two distinct groups: those with separate electrode compartment assemblies and those with non-separate electrode compartments. The non-separate electrode compartment has been successfully used by Kuikkola and Wagner (17). In their design, the electrodes were protected by flowing a purified inert gas over the cell in order to minimize the influence of one electrode on the other.

The separate electrode compartment configuration is used to essentially provide separate atmspheres in each compartment due to the requirements of the cell reaction and or to minimize cross interference between electrodes. Steele and Alcock (26) have successfully used such cell designs as those illustrated in Figures (3.1) and (3.2) and an excellent review of this topic is given in (27).

To ensure stable EMFs, the time for individual electrodes to equilibrate should be kept to a minimum. Since equilibration is dependant upon diffusion processes in solid phases, a small particle size can help keep equilibration times to a minimum. In practice this is

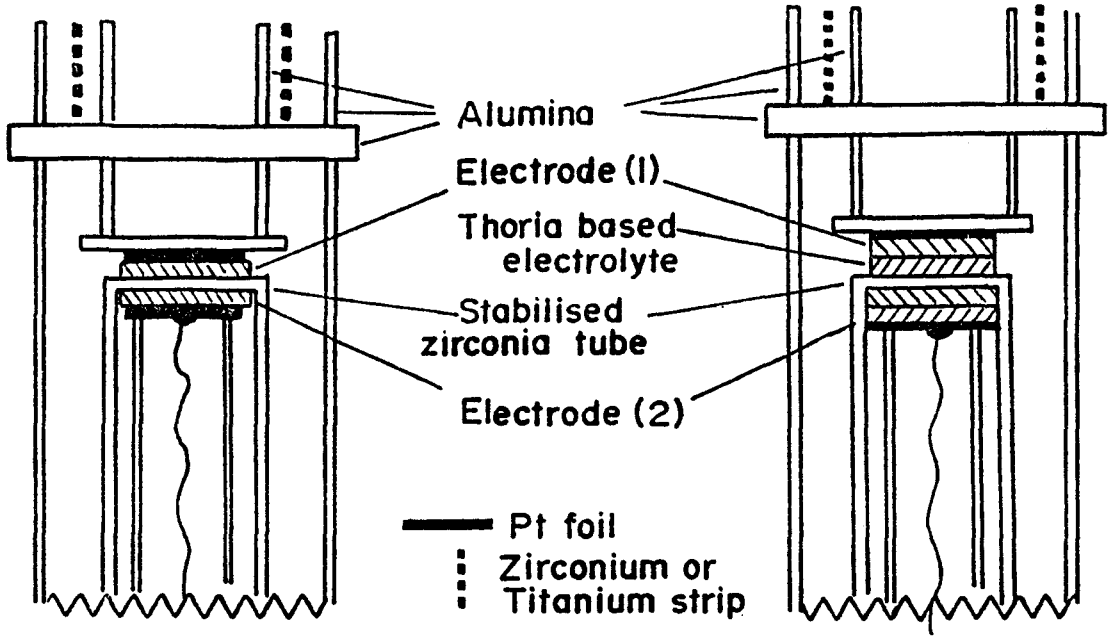

Figure 3.1: A solid electrolyte tube is used to separate the electrode assemblies (27).

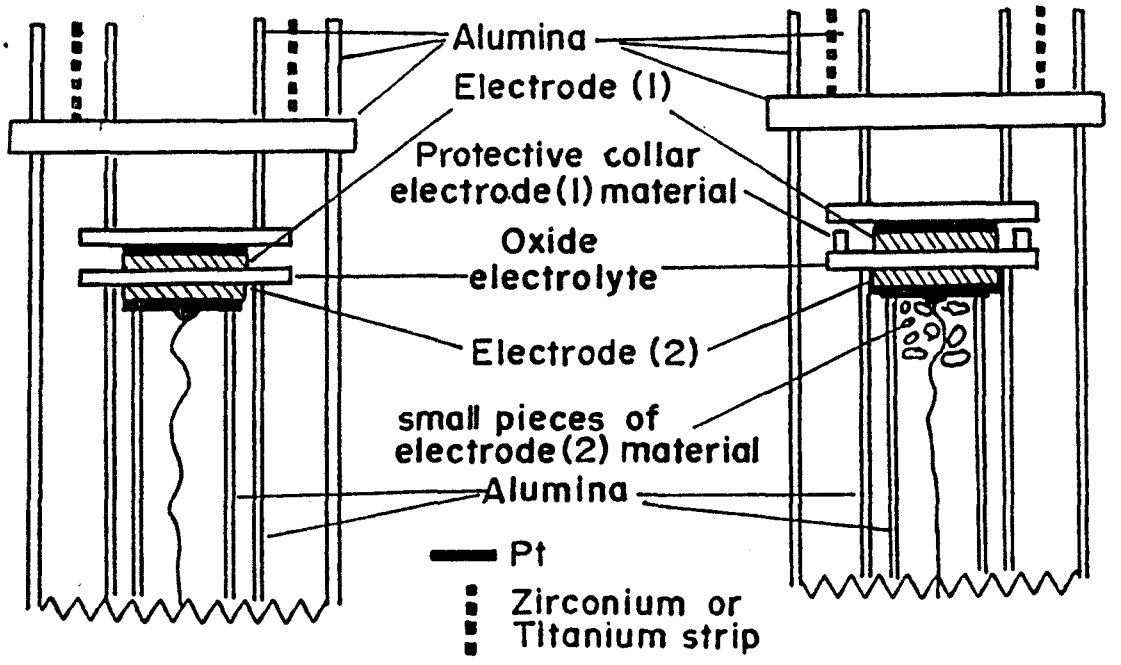

Figure 3.2: Separate electrode compartments are faciliated by using alumina tubes (27).

achieved by using an intimate mixture of fine powders which are pressed together into a dense disc or pellet.

The contacts between the electrode and the electrolyte and the electrode-lead contact are also critical. A good contact is achieved by ensuring smooth flat surfaces between the electrode-electrolyte interface and a lead material which will not react with the electrode. A good contact between the electrode and the electrolyte will also minimize any unwanted influence which the gaseous atmosphere may have on the equilibrium. For example, oxygen which is always present in a protective inert flowing gas atmosphere, may impose an unwanted potential on a low oxygen potential electrode.

CHAPTER 4

EXPERIMENTAL PROCEDURE

4.1 Summary of Galvanic Cells Used

EMF (electromotive force) measurements were made on the following reversible galvanic cells. The cells are broken into two distinct groups: the first group of cells (Group A) was used in the investigation of the thermodynamic properties of the ReSF compounds and the second group of cells (Group A) was used in the investigation of the characterization of the Caβ''-alumina type solid electrolyte.

Group A

$$Pt/Ag(s), Ag_2S(s), LaSF(s), LaOF(s)/CSZ/Air\ Pt \quad (4.1)$$

$$Pt/Ag(s), Ag_2S(s), CeSF(s), CeOF(s)/CSZ/Air/Pt \quad (4.2)$$

$$Pt/Ag(s), Ag_2S(s), PrSF(s), PrOF(s)/CSZ/Air/Pt \quad (4.3)$$

$$Pt/Ag(s), Ag_2S(s), SmSF(s), SmOF(s)/CSZ/Air/Pt \quad (4.4)$$

$$Pt/Ag(s), Ag_2S(s), TbSF(s), TbOF(s)/CSZ/Air/Pt \quad (4.5)$$

$$Pt/Ag(s), Ag_2S(s), HoSF(s), HoOF(s)/CSZ/Air/Pt \quad (4.6)$$

$$Pt/Ag(s), Ag_2S(s), YbSF(s), YbOF(s)/CSZ/Air/Pt \quad (4.7)$$

$$Pt/Ag(s), Ag_2S(s), YSF(s), YOF(s)/CSZ/Air/Pt \quad (4.8)$$

Group B

$$Pt/Cu(s), Cu_2S(s), CaS(s)/Ca\beta''\text{-alumina(a)}/Ag(s), Ag_2S(s), CaS/Pt \quad (4.9)$$

$$Pt/Cu(s), Cu_2S(s), CaS(s)/Ca\beta''\text{-alumina(b)}/Ag(s), Ag_2S(s), CaS/Pt \quad (4.10)$$

$$Pt/Cu(s), Cu_2S(s), CaS(s)/Ca\beta''\text{-alumina(c)}/Ag(s), Ag_2S(s), CaS/Pt \quad (4.11)$$

$Pt/Ni(s), NiO(s)/Ca\beta''\text{-alumina(b)}/Ni(s), NiF_2(s), CaF_2(s)/Pt$ (4.12)

$Pt/Ni(s), NiO(s)/Ca\beta''\text{-alumina(c)}/Ni(s), NiF_2(s), CaF_2(s)/Pt$ (4.13)

$Pt/CeO_2(s), CeF_3(s), CaO(\beta''\text{-alumina(a)}, CaF_2/CSZ/Air/Pt$ (4.14)

Note: "a", "b", "c" refer to the Caβ''-alumina compositions given in (4.2.2).

4.2 Materials

The materials used in this investigation are listed in table (4.1), together with the purity and source. The rare earth oxyfluoride and the rare earth thiofluoride compounds were prepared in this laboratory. The Caβ''-alumina solid electrolyte material was synthesised from purchased carbonate and oxide powders.

4.2.1 Preparation of the Rare Earth Oxyfluorides and Thiofluorides

The rare earth oxyfluoride compounds (except CeOF), were prepared by intimately mixing equi-molar proportions of the rare earth fluoride (ReF_3) and the rare earth sesqui-oxide (Re_2O_3) and heating them in the indicated atmospheres for 4-8 hours (see Table 4.2). The formation of the desired phases was confirmed by X-ray powder diffraction analysis before and after heating. The conditions necessary for synthesis of the various oxyfluorides are summarized below, in Table 4.2.

Table 4.1: Materials

Materials (mesh size)	Source	Purity
Calcium Sulphide (−325)	Cearac, Inc.	99.99
Calcium Fluoride (−325)	"	99.95
Copper (−325)	"	99.9
Copper Sulphide (−200)	"	99.9
Nickel (−325)	Ventron, Alpha	99.9
Nickel Oxide (−325)	Fisher Scientific	99.8
Nickel Fluoride (−325)	J.T. Backer Chem.	99.9
Silver (−325)	Ventron, Alpha	99.999
Silver Sulphide (−100)	Cerac, Inc.	99.9
La-Oxide (−325)	Cerac, Inc	99.9999
La-Sulphide (−200)	"	99.9
La-Fluoride (−325)	"	99.9
Ce-Fluoride (−325)	"	99.9
Ce-Oxide (−325)	"	99.9
Ce-Sulphide (−325)	"	99.9
Pr-Fluoride (−325)	"	99.9
Pr-Oxide (−325)	"	99.9
Pr-Sulphide (−200)	"	99.9
Sm-Fluoride (−325)	"	99.9
Sm-Oxide (−325)	"	99.999
Sm-Sulphide (−200)	"	99.9
Tb-Fluoride (−325)	"	99.9

Tb-Oxide (−325)	"	99.9
Tb-Sulphide (−200)	"	99.9
Ho-Fluoride (−325)	"	99.9
Ho-Oxide (−325)	"	99.9
Ho-Sulphide (−200)	"	99.9
Tb-Oxide (−325)	"	99.9
Tb-Sulphide (−200)	"	99.9
Ho-Fluoride (−325)	"	99.9
Ho-Oxide (−325)	"	99.9
Ho-Sulphide (−200)	"	99.9
Yb-Fluoride (−325)	"	99.9
Yb-Oxide (−325)	"	99.999
Yb-Sulphide (−200)	"	99.9
Y-Fluoride (−325)	"	99.9
Y-Oxide (−325)	"	99.9
Y-Sulphide (−325)	"	99.9
Calcium Carbonate	Ventron, Alfa	99.999
Magnesium Carbonate	Puratronic (JMC)	99.999
Aluminum Oxide (1-15 mic)	Ventro, Alpha	99.99
Platinum wire (10,20,30 mils)	Johnson Matthey	99.999

Table 4.2: Synthesis of ReOF Compounds

	ATMOSPHERE	TEMP (°C)	TIME (Hr)
LaOf	Air	850	8
YOF	Air	850	8
HoOF	Argon	850	8
YbOF	Argon	850	8
ErOF	Argon	1000	4
TbOF*	Argon	1000	4
PrOF	Argon	850	8
CeOF**	Hydrogen	850	8

* Terbium sesquioxide was prepared from its oxide Tb_4O_7 by heating in an hydrogen atomosphere at 1000°C for 4 hours.

** Cerium oxyfluoride was prepared from CeO_2:CeF_3, 2:1 ratio under a hydrogen atmosphere by the following reaction: $2CeO_2(s) + CeF_3(s) + H_2(g) = 3CeOF + H_2O(g)$

The rare earth thiofluorides were prepared by intimately mixing the appropriate rare earth fluoride and rare earth sesquisulfide in equimolar proportions and pressing the mixture into dense pellets. This technique was also used by Schmid and Hahn[7] who successfully synthesized LaSF, CeSF, and EuSF in their crystallographic investigations of these compounds. The pellets were then placed in quartz tubes which were evacuated to 5.0E-06 torr and sealed. The tubes were heated in a two stage cycle, first at 500°C for 24 hours and then at 800°C for an additional 48 hours. The phases present were verified by X-ray powder diffraction before and after heating. The diffraction data for these compounds are listed in Appendix II. The thiofluorides exhibited some striking colours, as indicated below:

COMPOUND	COLOUR
LaSF	Pastel yellow-green
YSF	Pastel green
CeSF	Brick red
HoSF	Pastel yellow
SmSF	Bright yellow
PrSF	Bright green
TbSF	Green
YbSF	Beige

4.2.2 Preparation of the Calcium β''-aluminas

Caβ''-alumina was synthesized with the compositions listed in Table 4.3.

Table 4.3: Composition of Caβ''-Aluminas

COMPOSITION	CaO	MgO	Al_2O_3	PHASES
(a)	1.0	0.6	6.0	β''
(b)	1.0	0.8	8.0	β'', $MgO.Al_2O_3$ α-Al_2O_3
(c)	1.0	1.2	6.0	β'', $MgO.Al_2O_3$ $CaO.2Al_2O_3$

These compositions were selected from Kumar's[16] investigation of the Caβ″-alumina phase field of the CaO-MgO-Al_2O_3 ternary system. Kumar directly sintered ten compositions which were randomly distributed over the relevant range of the Caβ″-alumina phase field. He chose to investigate in more detail the single phase Caβ″-alumina material and characterized the behaviour of this material as a solid electrolyte.

In order to evaluate the potential of the Caβ″-alumina solid electrolyte as a possible high temperature calcium or oxygen probe, three phase compositions b and c, which are the two three phase compositions found by Kumar, have been chosen in this investigation for further characterization.

These solid electrolyte materials were made from high purity calcium carbonate, magnesium carbonate and alumina powders. The subsequent processing of these powders was found to be very critical in achieving the desired physical and chemical properties of the final product.

A flow chart of the processing is given in Table 4.4, however, the following additional precautions should be given due consideration:

1. The aforementioned materials are very susceptible to atmospheric humidity. It was found virtually impossible to produce sound pellets on hot humid days when the ambient exterior temperature was above 21°C. Hence the required materials were processed when the ambient conditions were favourable. The processed materials were then stored in cool dry dessicators.

2. Achievement of high final densities ranging from 3.87 to 3.90 gm/cc was found to be imperative to the successful operation of these electrolytes. In order to realize this, high green densities are essential. All other conditions being equal, it was found that isostatic pressing between 40,000-55,000 psi is sufficient to produce consistent final densities.

3. Finally, it was found that composition "b" (see Table 4.2.2) had the poorest sintering characteristics and that compositions "a" and "c" consistently had higher final densities than the former for a given time and temperature heating cycle.

4.3 Cell Design

Two cell configurations were used in this investigation. The first type used exclusively in the investigation of the rare earth thiofluorides is designated as cell design "A". The second configuration was used in the investigation of the Caβ''-aluminas and is designated as cell design "B".

4.3.1 Cell Design "A"

This cell design utilized a CSZ (calcia stabilized zirconia) closed end tube purchased from Corning Inc. which measured 300 mm by 10 mm dia. with a 1 mm wall. Two concentric alumina tubes were placed inside the CSZ tube. The innermost one was a sheath for a platinum lead which was led down the centre of the closed end tube. The second alumina tube provided a channel for a dynamic inert gas atmosphere to be introduced over the inner electrode. In this design the anode and cathode compartments are totally separated from each other by the electrolyte tube. The CSZ tube was sealed off with rubber seals at the top and the concentric alumina tubes which extended longer than the electrolyte tube were also sealed off with provisions to introduce an inert gas, as shown in Figure (4.1). An additional platinum wire was led down the outside of the CSZ tube which was used to make contact with the exterior electrode which in this case was air.

TABLE 4.4: Preparation of Calcium β''-Alumina Powders

Weighing of appropriate amounts of $CaCO_3$, $MgCO_3$, Al_2O_3, powders.

10 hrs. vibratory mixing in high purity acetone with alumina grinding balls, followed by 144 hrs rotary ball mill grinding.

Evaporation of acetone, 48 hrs at room temperature followed by 8 hrs at 200°C.

Powder is then hand ground and placed in alumina crucibles for calcination at 1000°C for 100 hrs.

10 hrs vibratory mixing in high purity acetone with alumina grinding balls, followed by 144 hrs rotary ball mill grinding.

Evaporation of acetone, 48 hrs at room temperature followed by 8 hrs at 200°C.

Powder is then hand ground and pressed uniaxially into 12 mm dia. pellets at 4000 psi. These pellets are then iso-statically pressed at 40,000 to 50,000 psi.

The pellets are sintered at 1600°C for 6 hrs or 1650°C for 4 hrs.

The inner electrode consisted of the desired phases in powder form thoroughly mixed and compacted at the bottom of the CSZ tube in intimate contact with the inner electrode. The inert gas which consisted of purified argon was continuously flushed through the inner compartment at the rate of 20 cc per minute.

4.3.2 Cell Design "B"

In this cell design the electrodes are separated by a solid electrolyte in the form of a disk shaped pellet, roughly 10 mm in diameter and 2.5 mm thick. The desired phases for the electrodes were mixed together and pressed into a pellet which was 6 mm in diameter and 4 mm thick. The compositions of the electrodes used are summarized in Table (4.5) below. The cell, consisting of two electrode pellets separated by the solid electrolyte pellet, was placed in a quarz tube as illustrated in Figure (4.2). Platinum leads were placed in contact with the electrodes and a good electrode-electrolyte contact was assured by pressing the assembly together with a spring loaded alumina push rod. The entire assembly was then placed inside a quartz tube, which sealed off the cell from the atmosphere, and an inert gas was passed over the cell assembly.

Table 4.5: Electrode Compositions

Components	Weight Ratios
Ag, Ag_2S, ReSF, ReOf	4:1:2:1
Cu, Cu_2S, CaS	3:1:1
Ag, Ag_2S, CaS	3:1:1
Ni, NiF_2, CaF_2	3:1:1
Ni, NiO	3:1

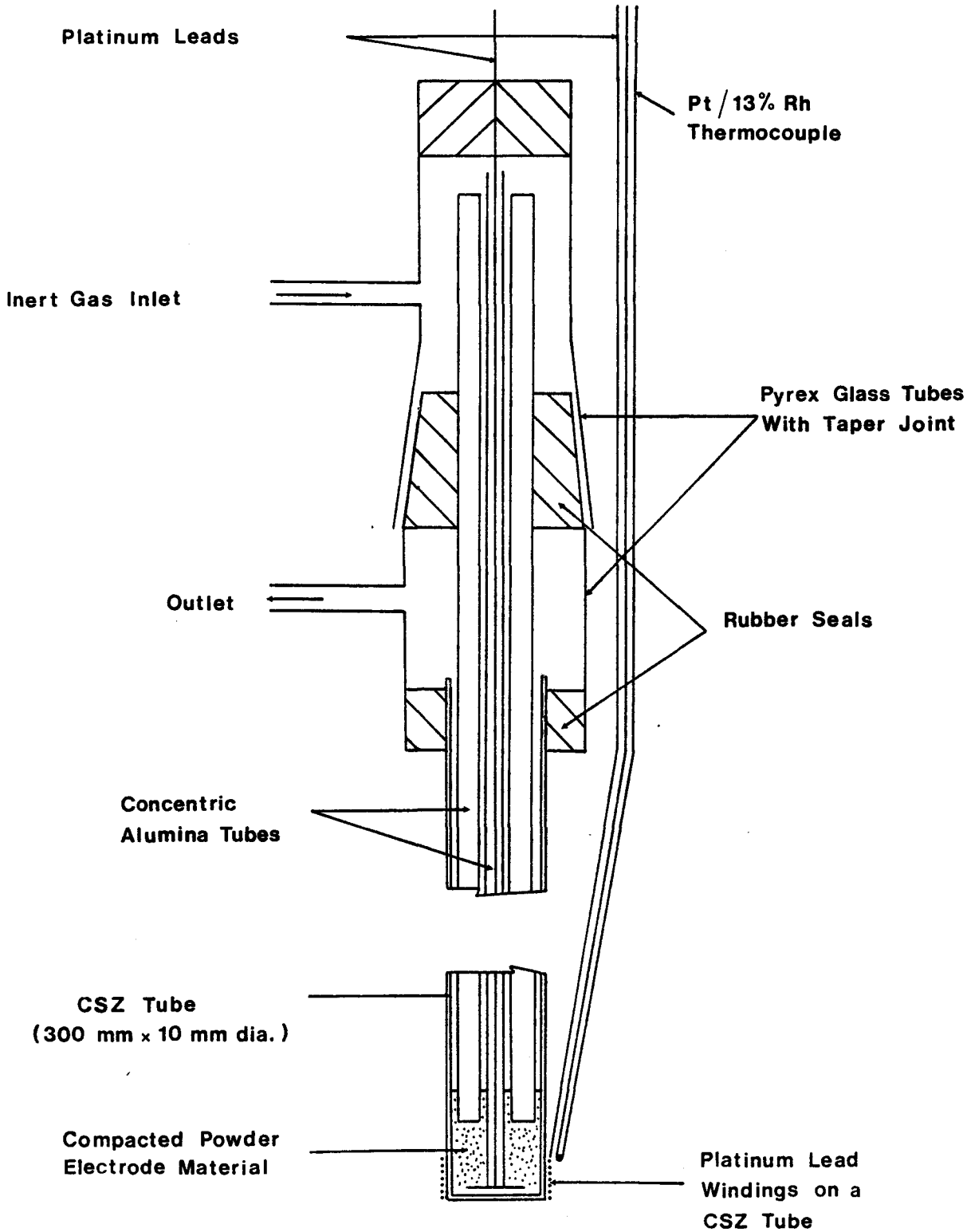

Figure 4.1: Cell design "A" used in the investigation of the rare earth thiofluorides.

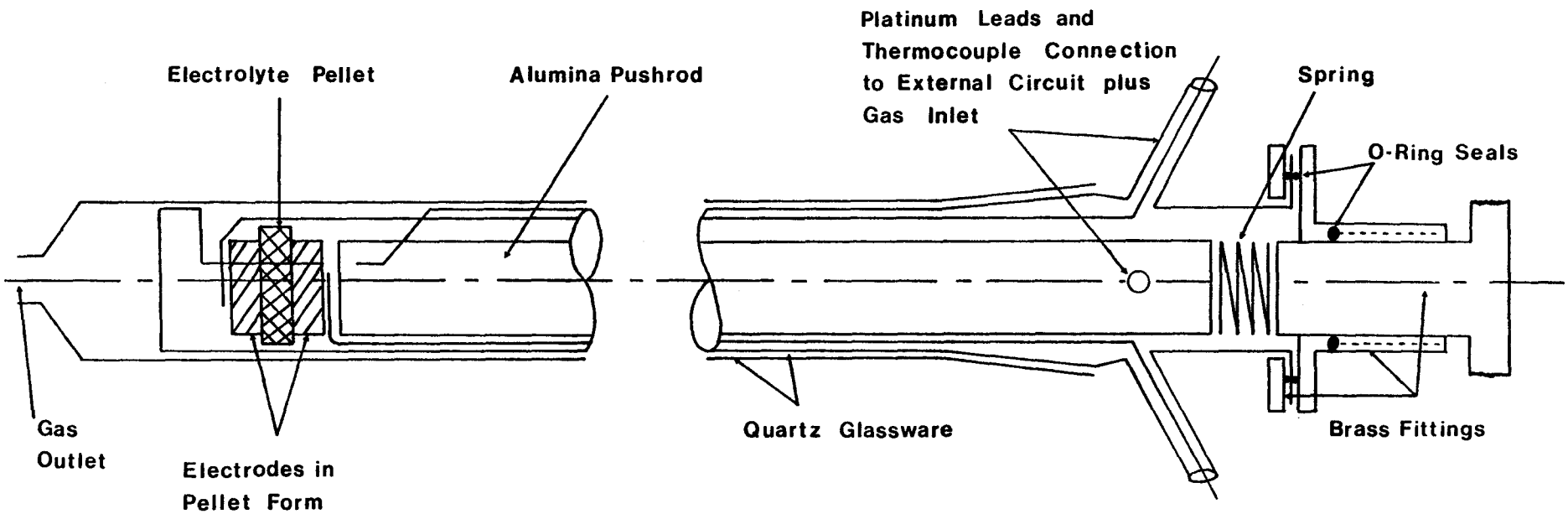

Figure 4.2: Cell design "B" used in the investigation of the Caβ'' aluminas.

4.4 Operation and Measurement of Cells

The cells were heated in a horizontal platinum-rhodium wound furnace which was controlled to $\pm 1°C$ by a Barber-Coleman proportional controller and the temperature measured with a platinum-13% rhodium thermocouple. In order to reduce any induced currents, the cells were placed inside a grounded inconel tube. The cells were generally heated for at least 8 hrs before any measurements were taken in order to ensure equilibration of the electrodes. The cell EMFs were measured with a Keithley 615 digital electrometer which has an input impedance of 1.0E14 ohms. The cell was considered to be at equilibrium when the EMF value was stable for a period of 30 minutes and, when a small current, was passed through the cell in either direction, the cell would return to its original value. The cells were generally operated for a time period of 38 to 80 hrs depending upon the behaviour and equilibriation time of the cell. The influence of the flowing inert gas on the cell was checked by varying the flow rates to see if the EMFs remained stable and unaffected.

CHAPTER 5

EXPERIMENTAL RESULTS

5.1 EMF Results of Group A Cells

The coexistence of the phases in the electrodes was verified by X-ray analysis before and after cell measurements had been taken. The presence of the original phases and the appearance of no additional phases was taken as confirmation that the phases present coexisted under the prevailing experimental conditions. The EMF data is presented in Appendix III and plotted as a function of temperature for one experimental cell in Figures (5.1) to (5.8). The anode oxygen partial pressures which were present in the group A cells is plotted in Figure (5.9) along with the Ag_2S-Ag_2SO_4 equilibria, establishing the stability of Ag_2S in the anode compartment for this group of cells.

5.2 Results of Group B Cells

Cells 4.9, 4.10 and 4.11 were set up to establish the reversibility of the manufactured pellets to Ca ions. This cell is identical to the one used by Kumar (16) and for comparison the thermodynamic data from Mills (28) was used to predict the EMFs. The coexistence of the anode and cathode phases was verified by Kumar (29).

Cells 4.12, 4.13 and 4.14 were designed to measure the CaO activities in the Caβ''-alumina compositions investigated. Cells 4.12 and 4.13 are similar to the cell (given below) used by Choudhury (30) in which he determined the Na_2O activity in the alpha-beta alumina coexistence.

$$Pt/Ni, NiF_2, NaF/\text{alpha-beta alumina}/Cu, Cu_2O/Pt \qquad (5.1)$$

The EMF's for these cells are listed in Appendix III and the data for the experimental cells are plotted in Figures (5.10) through (5.13).

Table 5.1

Summary of EMF Data for Cells 4.1-4.14

Cell	Least squares Fit EMF (mv) = [A(mv) + B(mv) T(k)] A	B	Std. Error EMF (mv)
4.1	1238	−0.1962	1.9
4.2	1195	−0.1417	1.7
4.3	1237	−0.1452	2.0
4.4	1317	−0.1931	3.8
4.5	1513	−0.3156	1.3
4.6	1564	−0.4023	3.9
4.7	1364	−0.1227	1.5
4.8	1450	−0.1774	1.7
4.9	192.2	0.0593	3.4
4.10	172.1	0.0793	4.8
4.11	186.4	0.0644	4.6
4.12	120.4	0.5321	4.7
4.13	143.7	0.3039	4.1
4.14	1599	−0.5139	4.7

Figure 5.1: Variation of EMF with temperature for cell 4.1.

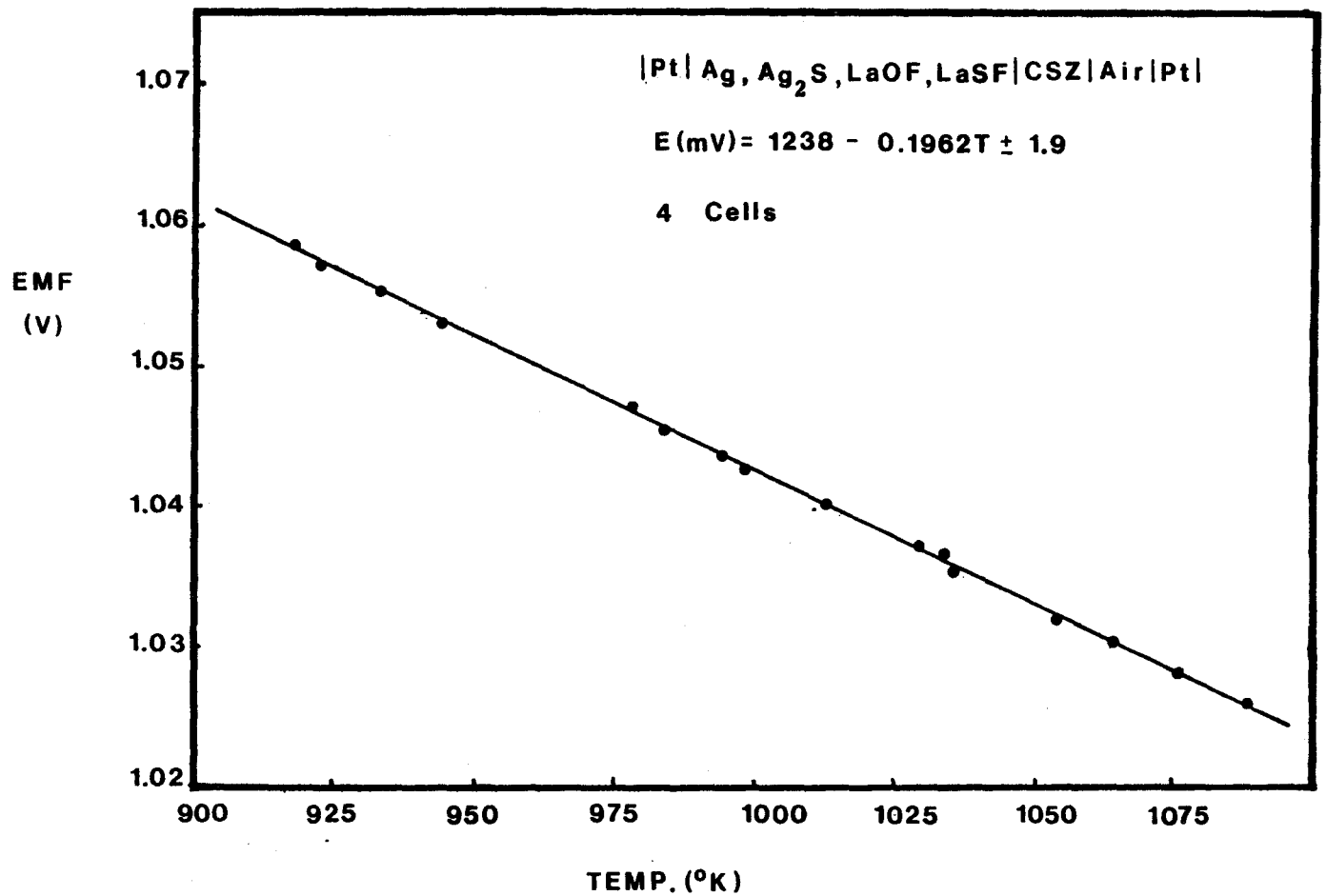

Figure 5.2: Variation of EMF with temperature for cell 4.2.

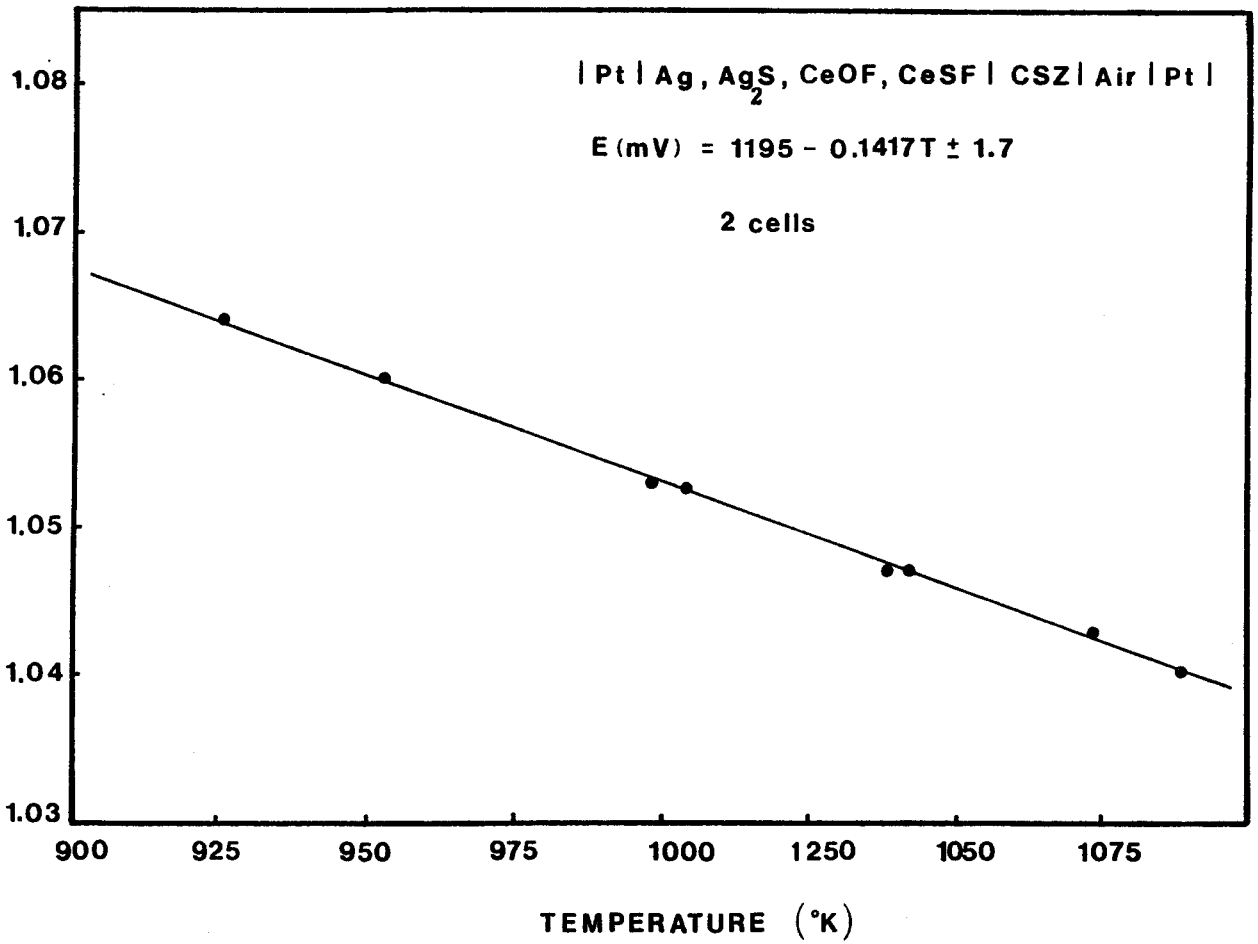

Figure 5.3: Variation of EMF with temperature for cell 4.3.

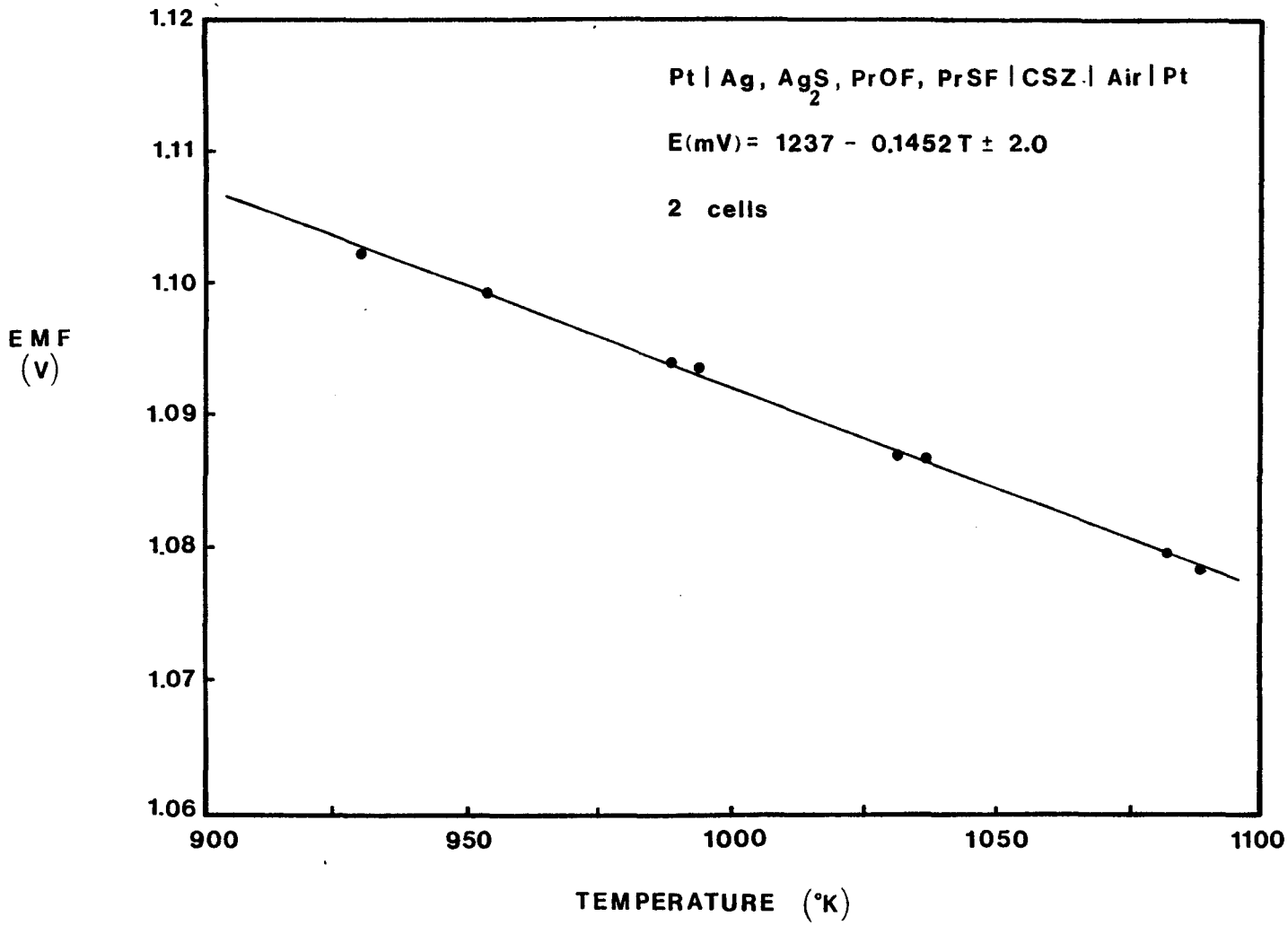

Figure 5.4: Variation of EMF with temperature for cell 4.4.

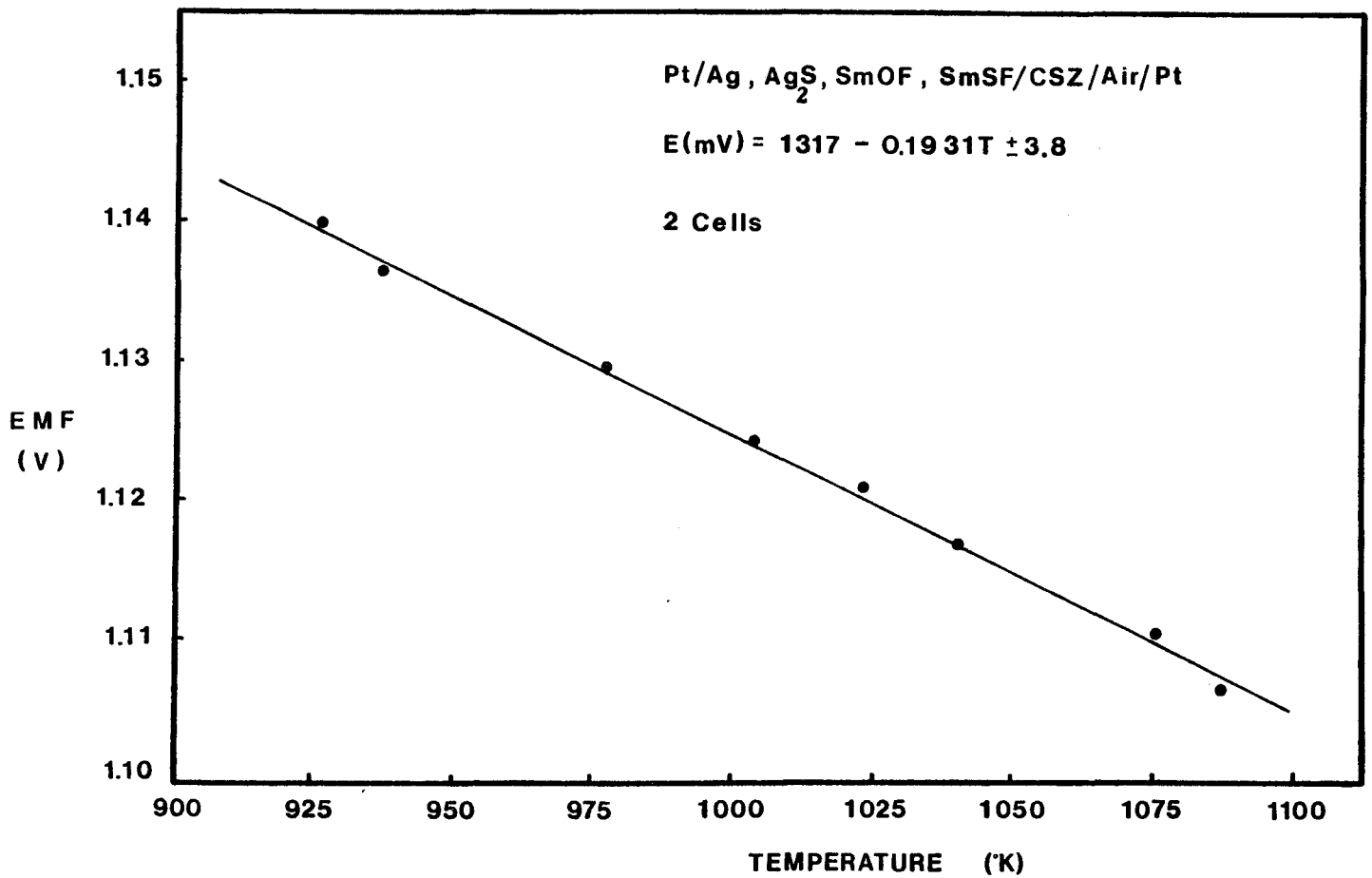

Figure 5.5: Variation of EMF with temperature for cell 4.5.

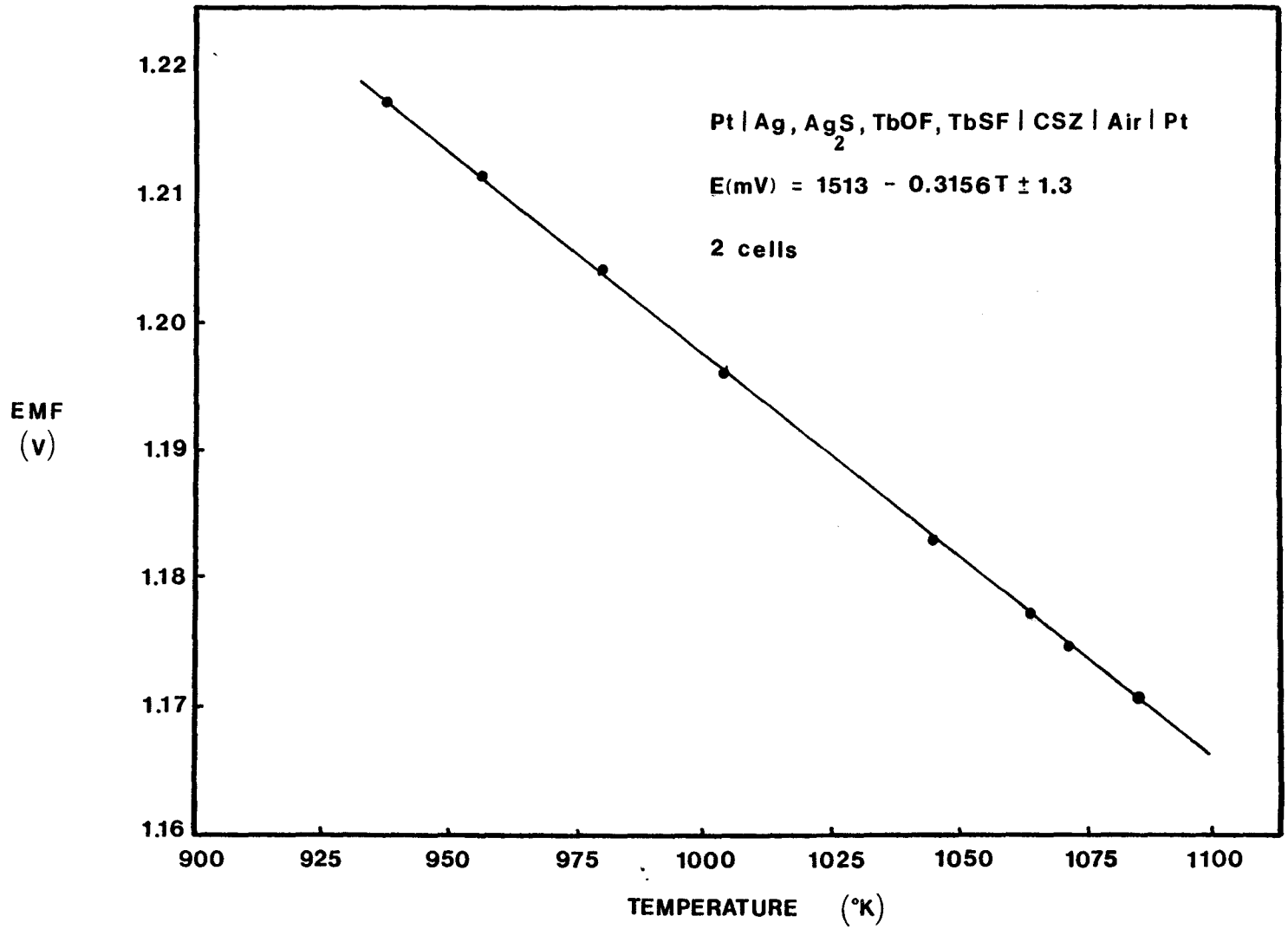

Figure 5.6: Variation of EMF with temperature for cell 4.6.

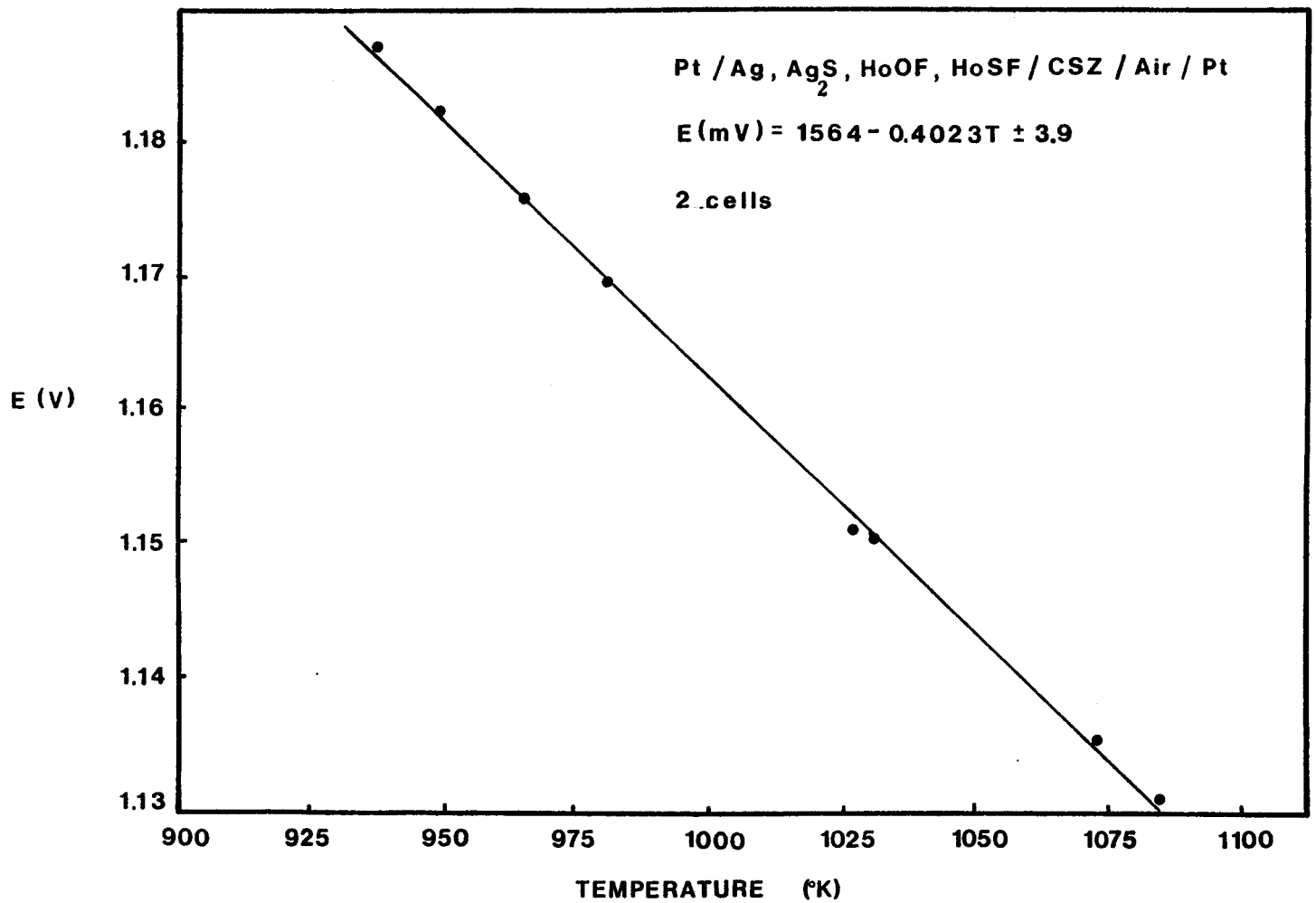

Figure 5.7: Variation of EMF with temperature for cell 4.7.

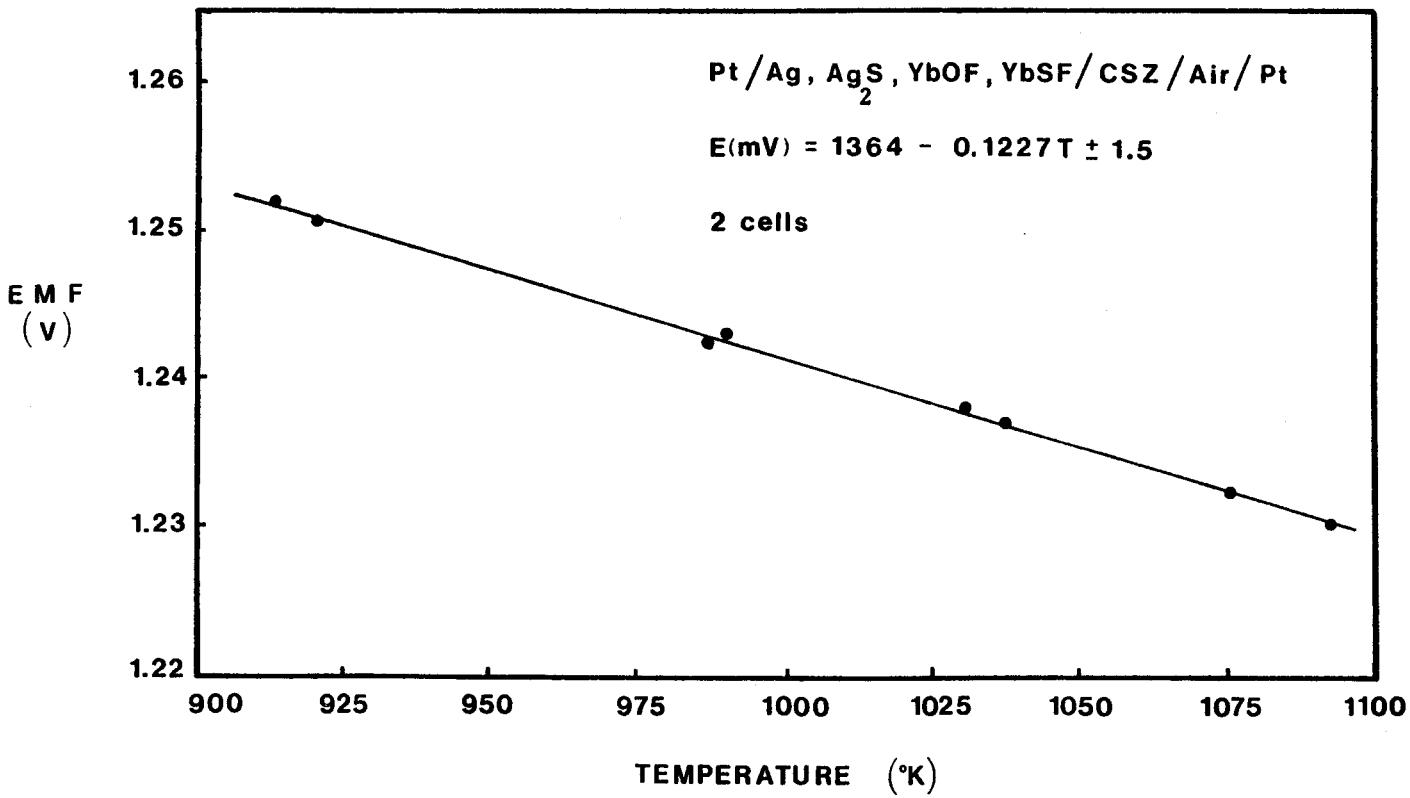

Figure 5.8: Variation of EMF with temperature for cell 4.8.

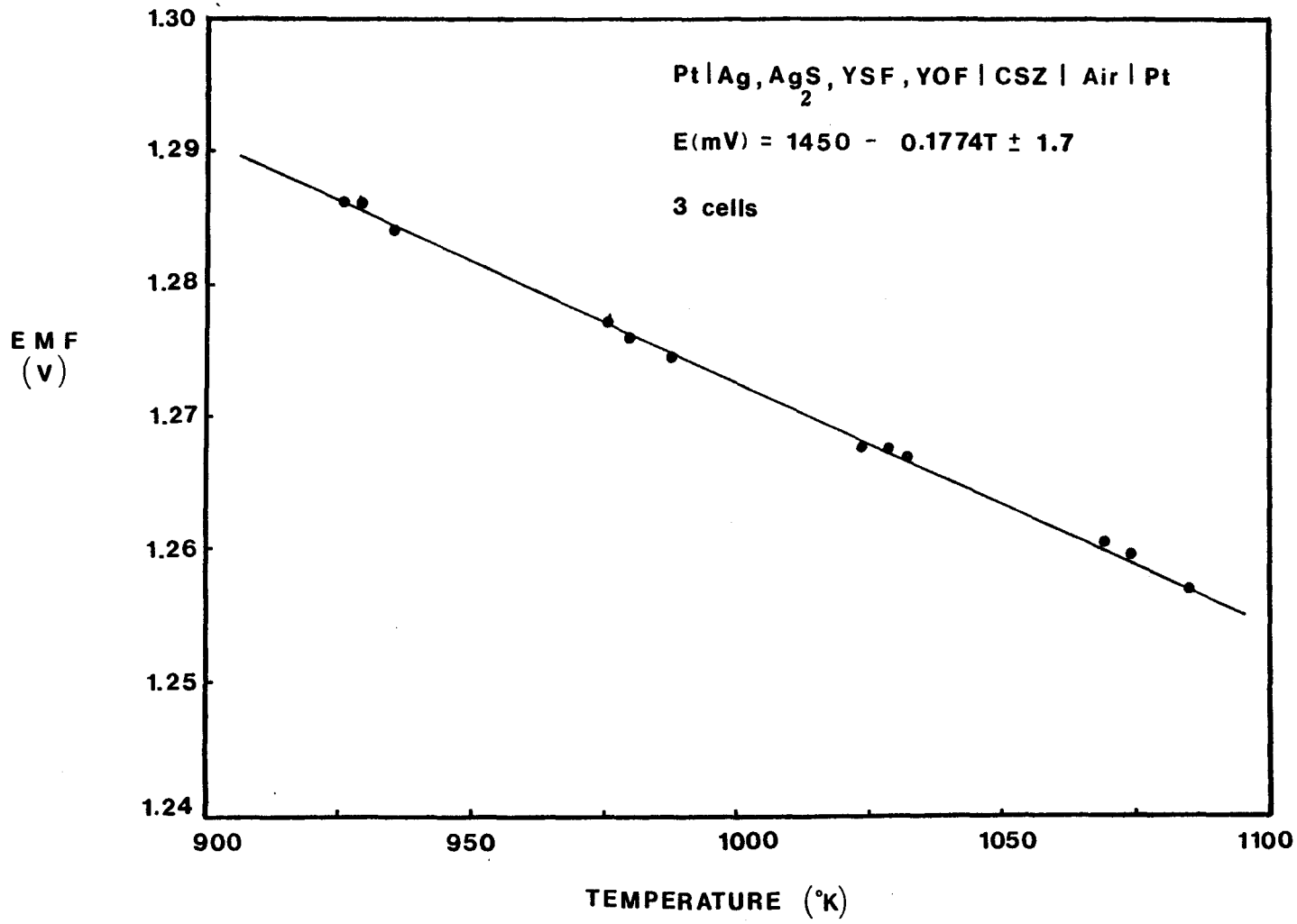

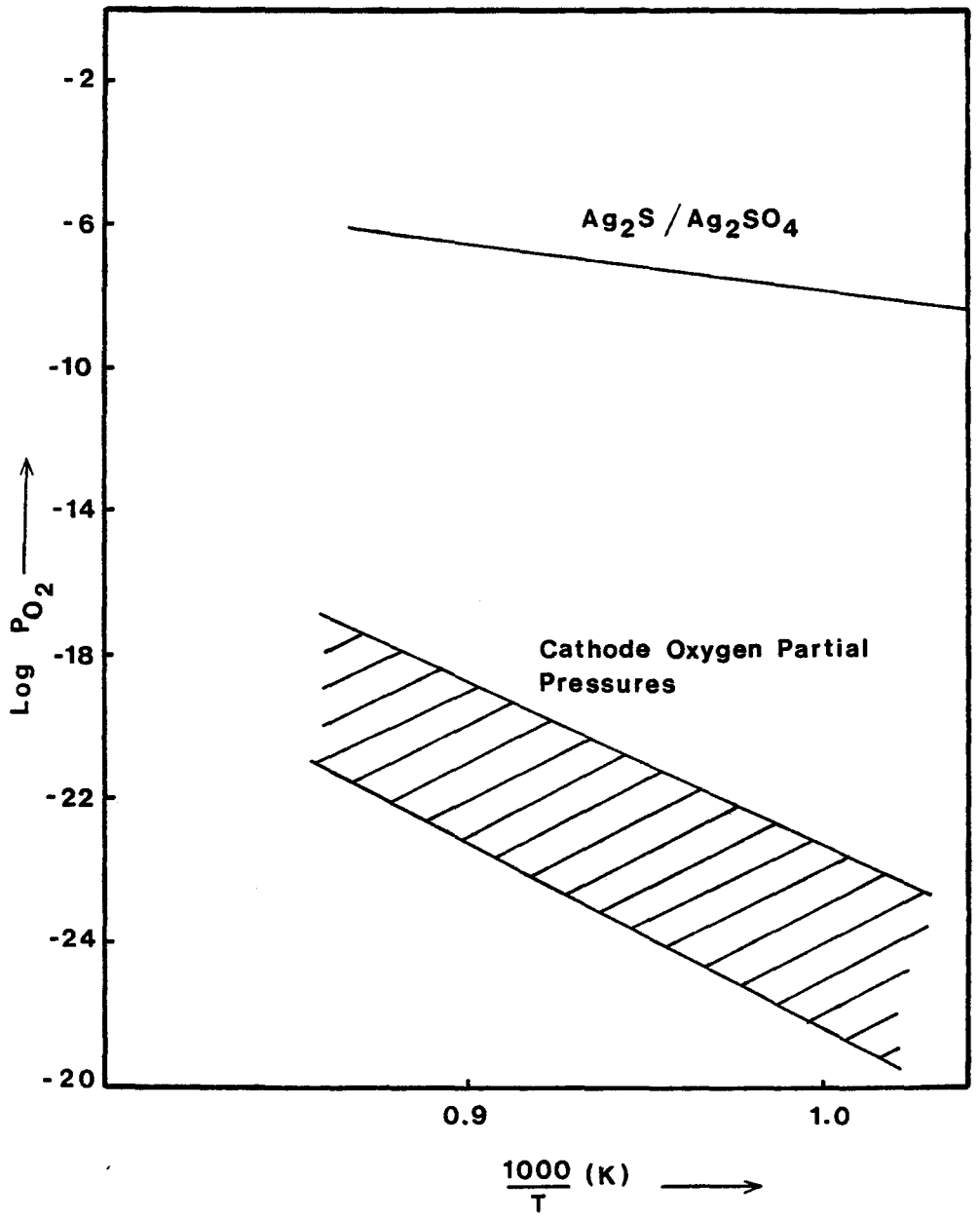

Figure 5.9: Cathode Oxygen Partial Pressures in Relation to the Ag_2S/Ag_2SO_4 Equilibrium

Figure 5.10: Variation of EMF with temperature for cells 4.9(a), 4.10(b), 4.11(c).

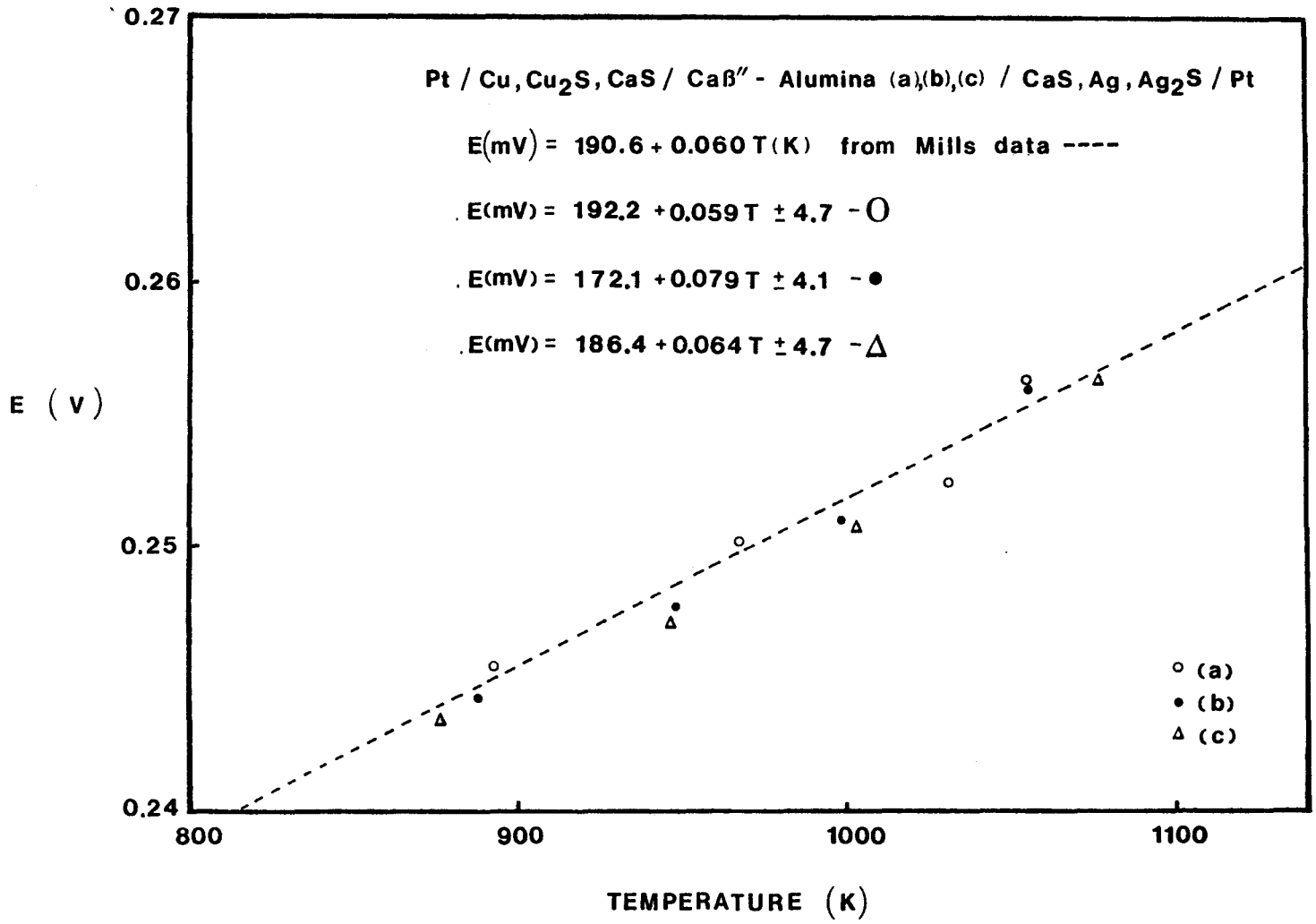

Figure 5.11: Variation of EMF with temperature for cell 4.12.

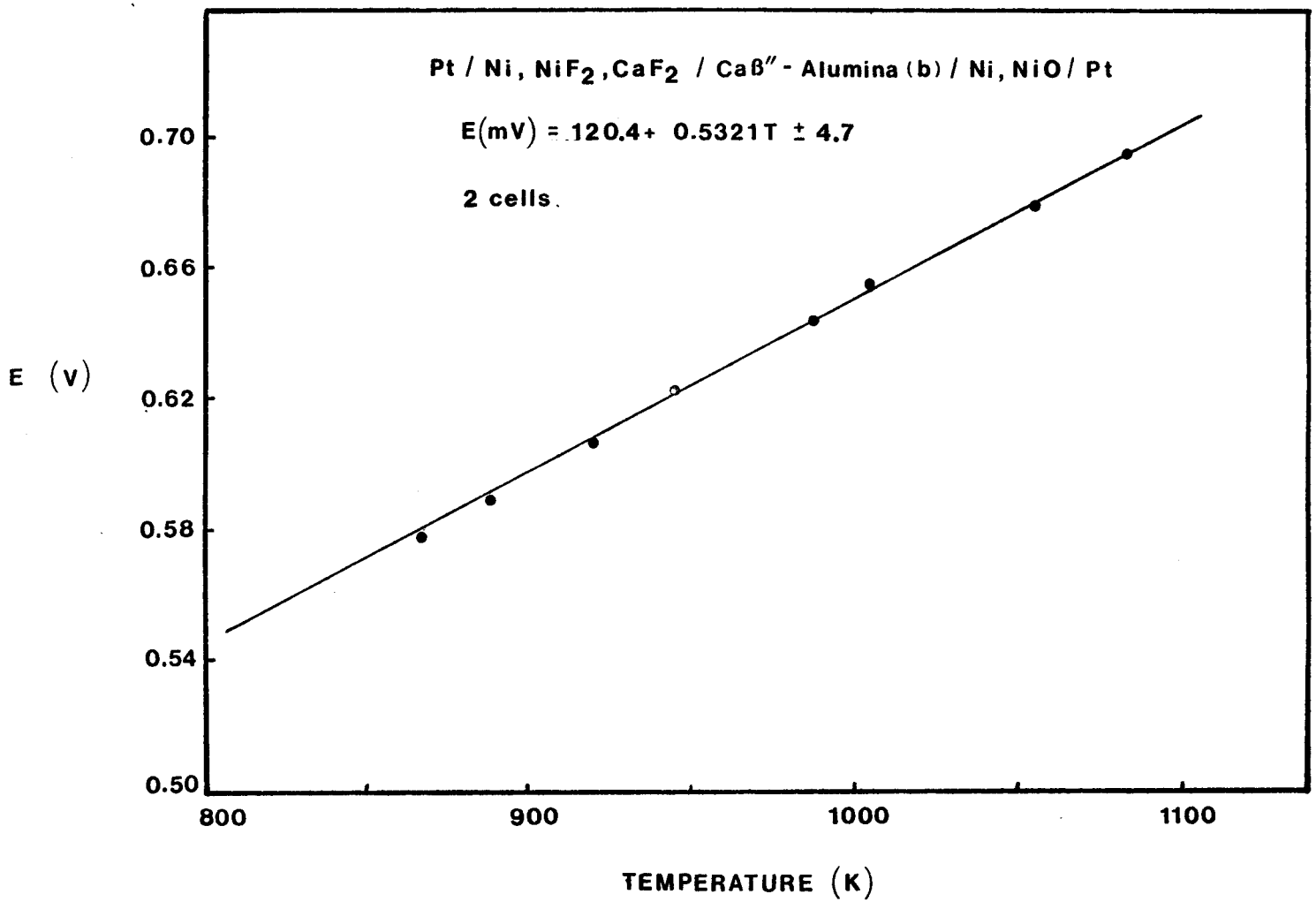

Figure 5.12: Variation of EMF with temperature for cell 4.13.

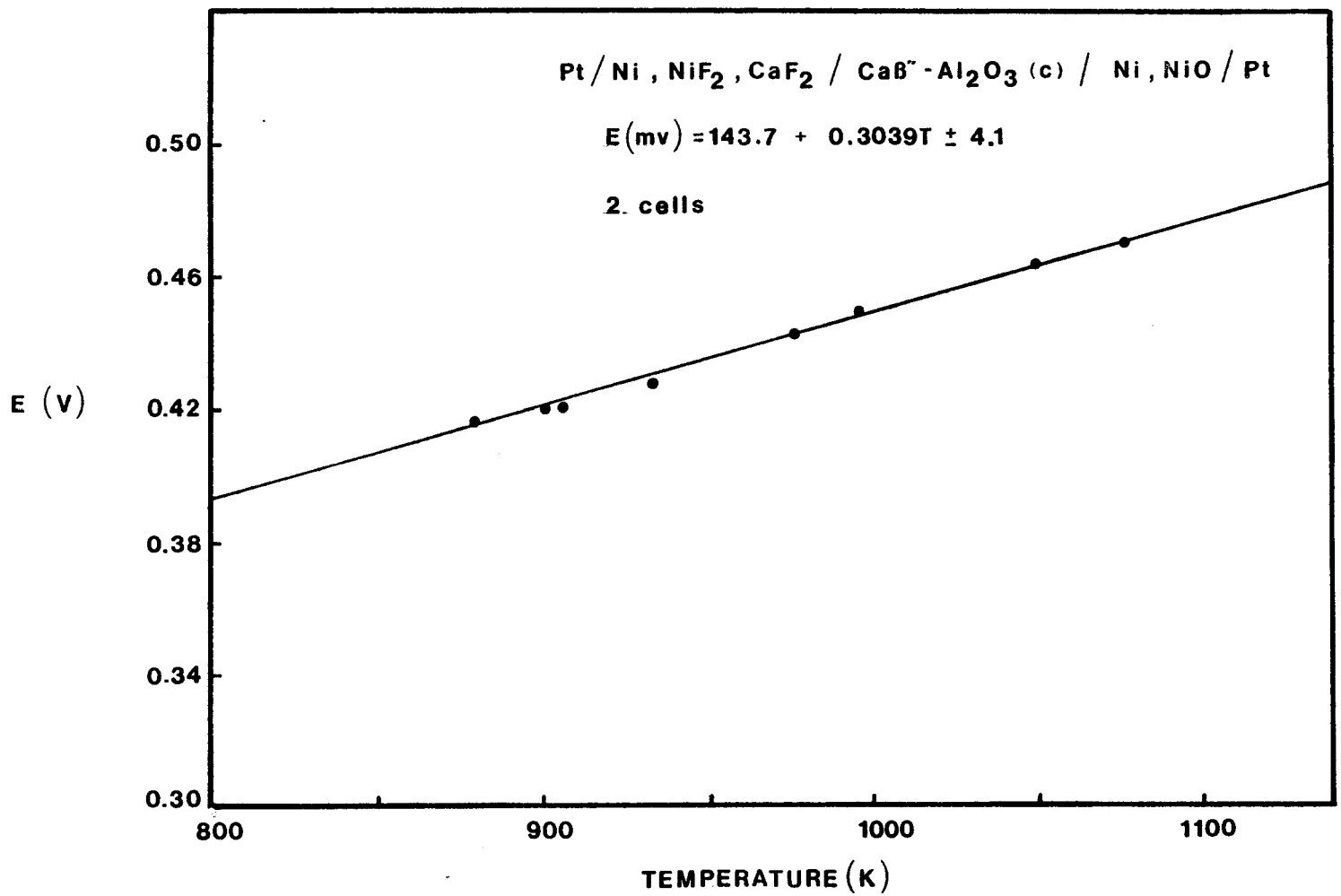

Figure 5.13: Variation of EMF with temperature for cell 4.14.

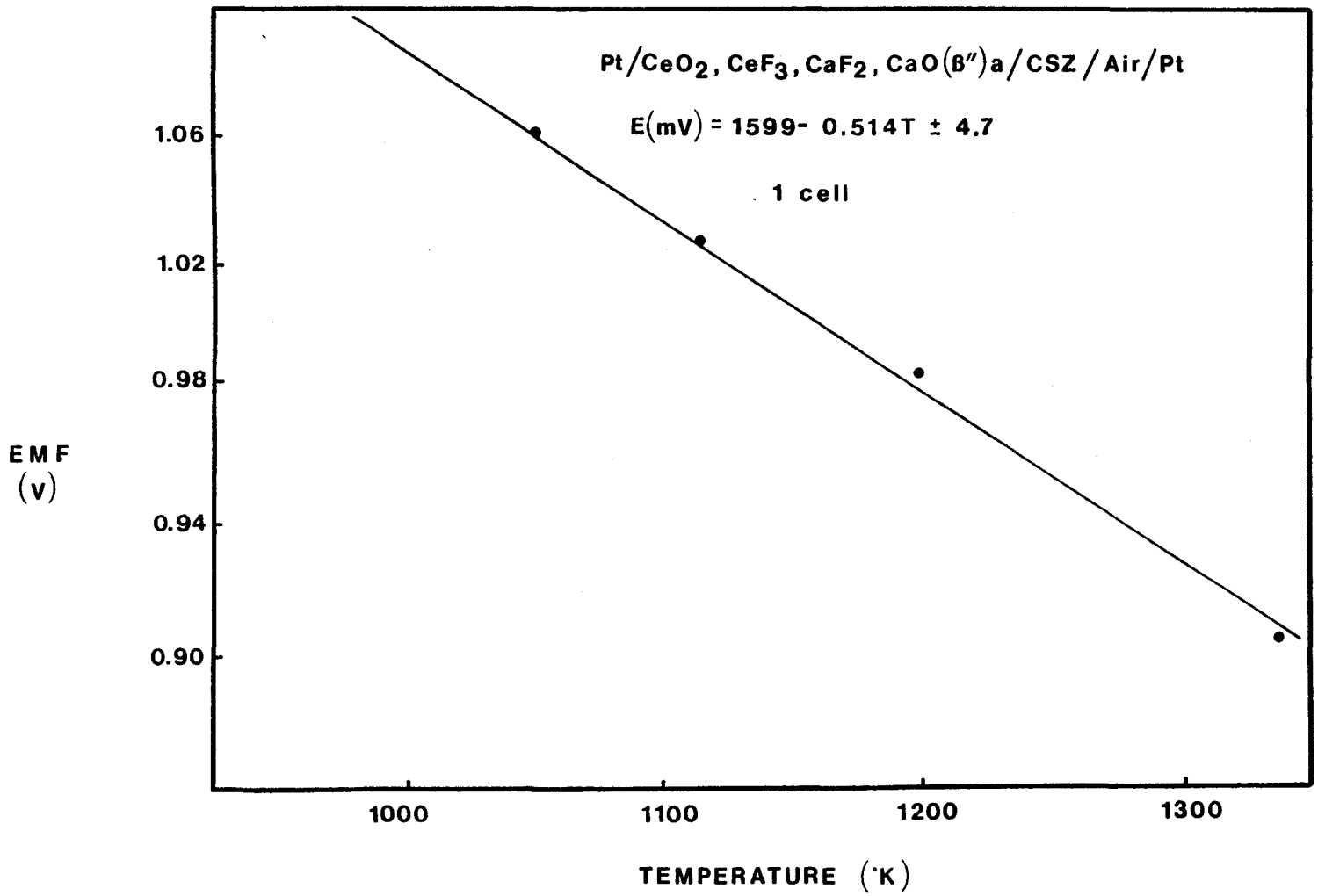

CHAPTER 6

ANALYSIS OF RESULTS AND DISCUSSION

6.1 Treatment of Group A Cell Data

The galvanic cells in Group A are similar in that the anodic and cathodic reactions differ only in the rare earth element which is under consideration. This allows the treatment of the results of these cells to be handled in a similar fashion. A general treatment for the analysis of the results obtained from these cells is given here. The theory for the evaluation of cell data has been presented in Chapter 3. The anodic, cathodic and virtual cell reactions and also the determination of the free energies of formation and reaction are given below:

For the generalized cell:

$$Pt/Ag, Ag_2S, ReOF, ReSF/CSZ/Air/Pt \tag{6.1}$$

The anode reaction is

$$ReSF + 2Ag + O^{=} = Ag_2S + ReOF + 2e^{-} \tag{6.2}$$

The cathode reaction is:

$$2e^{-} + \frac{1}{2}O_2 = 0^{=} \tag{6.3}$$

and the virtual cell reaction is:

$$ReSF + 2Ag + \frac{1}{2}O_2(cath) = Ag_2S + ReOF \tag{6.4}$$

The standard Gibbs free energy change for the virtual cell reaction is given by:

$$-nFE = RT\,\ell n\,K + \Delta G^0(6.4) \tag{6.5}$$

From equation 6.4

$$nFE = \frac{1}{2}\,RT\,\ell n\,PO_2(cath) + \Delta G^0_{ReSF} - \Delta G^0_{Ag_2S} - \Delta G^0_{ReOF} \tag{6.6}$$

where $PO_2(c) = 0.21$ (atm).

Substituting relationship 6.5 into 6.6 and solving for $\Delta G^0(ReSF)$ one can write the following expression:

$$\Delta G^0(ReSF) = nFe - \frac{1}{2} RT\, \ell n\, PO_2(cath) + \Delta G^0(ReOF) + \Delta G^0(Ag_2S) \qquad (6.7)$$

The data used in the calculation of equation (6.7) is listed in Table 6.1 and the results obtained from this calculation are presented in tabular form in Table 6.2.

The desulphurizing potential of the rare earth oxyfluorides was evaluated by calculating the free energy change associated for the conversion of the rare earth oxyfluoride to the rare earth thiofluoride. This was determined by subtracting equation (6.8) below, from the virtual cell reaction eqn. (6.4) yielding the desired relationship (6.9).

$$2Ag + \frac{1}{2} S_2 = Ag_2S \qquad (6.8)$$

$$ReSF + \frac{1}{2} O_2 = ReOF + \frac{1}{2} S_2 \qquad (6.9)$$

The standard Gibbs free energy change for reaction (6.9) is given by the following relationship:

$$\Delta G^0(6.9) = -nFe + \frac{1}{2} RT\, \ell n\, PO_2(cath) - \Delta G^0(Ag_2S) \qquad (6.10)$$

The results obtained from equation (6.10) are presented in Table 6.3 and summarized in Figure 6.1.

Table 6.1: Summary of Thermodynamic Data Used for Cells 4.1 to 4.8

Compound (ref.)	Standard Free Energy of Formation $\Delta G^\circ = A + BT(K)$ [cal]		Error ±cal	Temp. Range (K)
	"A"	"B"		
Ag_2S (43)	−20990	8.26	2400	452-1115
LaOF (35)	−292239	43.76	1584	900-1100
YOF (35)	−289987	36.12	2559	930-1245
TbOF (35)	−290887	42.01	2905	958-1167
CeOF (35)	−281858	35.38	2159	1077-1277
PrOF (35)	−290688	44.02	4676	978-1068
SmOF (35)	−286437	41.17	1430	951-1094
HoOF (35)	−290964	33.77	1543	882-1132
YbOF (35)	−286155	43.42	2479	898-1058

Values in calories may be converted to joules by multiplying by 4.182.

Table 6.2: Standard Free Energy of Formation of ReSF Compounds

Compound	Standard Free Energy of Formation $\Delta G^\circ = A + BT(K)$ [cal]		Error + – cal	Temp. Range (K)
	"A"	"B"		
LaSF	– 256120	44.52	2884	919-1088
CeSF	– 247722	38.65	3235	925-1086
PrSF	– 254615	47.13	5261	931-1083
SmSF	– 246674	42.04	2811	923-1084
TbSF	– 242082	37.26	3773	933-1085
HoSF	– 239807	25.02	2870	939-1087
YbSF	– 244316	47.57	3457	913-1090
YSF	– 244088	37.75	3515	925-1087

Values in calories may be converted to joules by multiplying by 4.182.

Table 6.3: Standard Free Energy Change for the Reaction

$$ReSF + 1/2O_2 = ReOF + 1/2S_2$$

Rare Earth	Standard Free Energy Change $\Delta G° = A + BT(K)$ [cal]		Error + – cal
	"A"	"B"	
La	–36119	+0.76	2410
Ce	–34136	–3.27	2409
Pr	–36073	–3.11	2411
Sm	–39763	–0.90	2420
Tb	–48805	+4.75	2408
Ho	–51157	+8.75	2421
Yb	–41839	–4.15	2408
Y	–45899	–1.63	2410

Values in calories may be converted to joules by multiplying by 4.182.

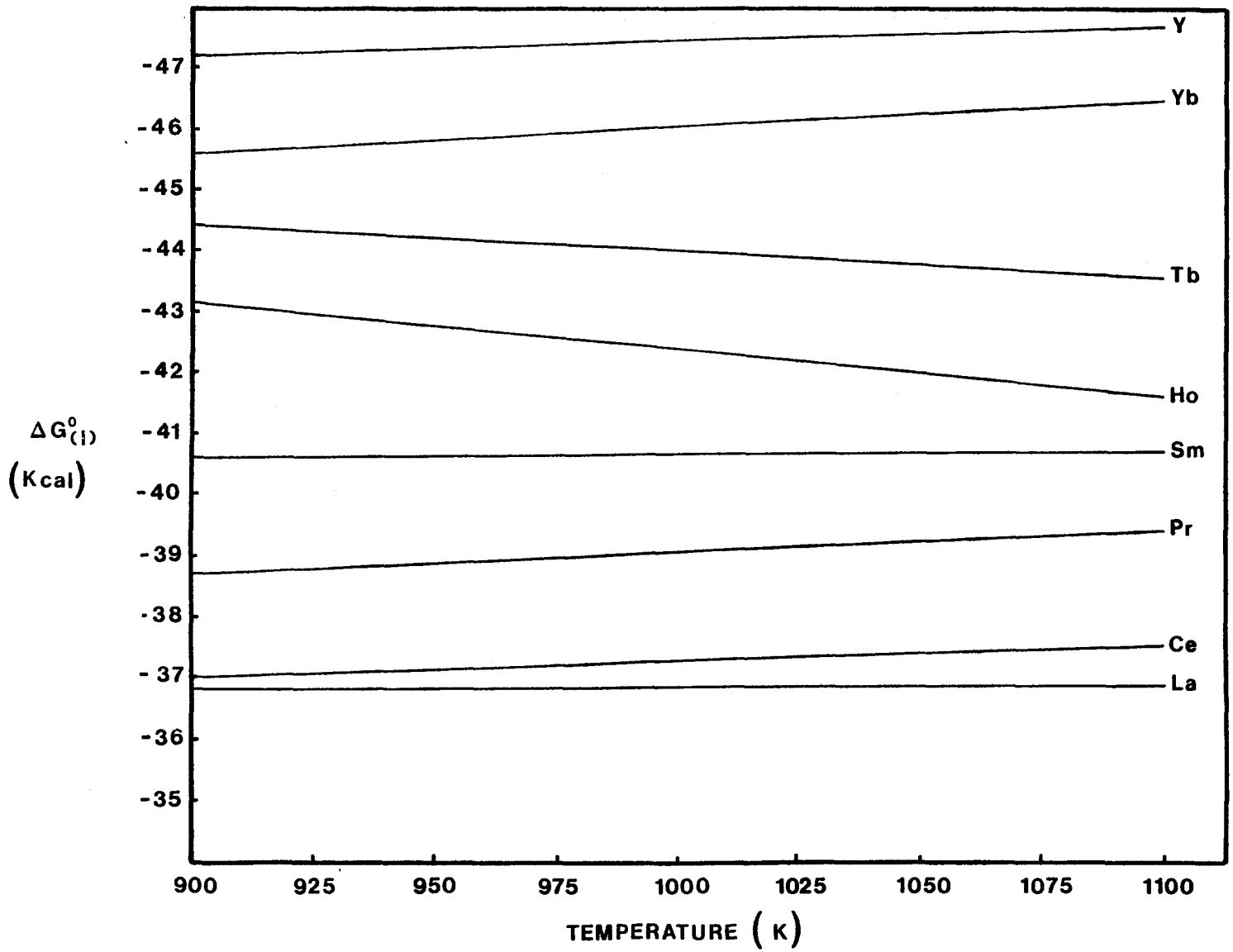

Figure 6.1: **The Standard Free Energy Changes For The Reactions:**

$$ReSF + {}^{1}/_{2}O_2 \rightarrow ReOF + {}^{1}/_{2}S_2$$

6.2 Treatment of Group B Cell Data

Cells 4.9, 4.10, and 4.11 were used to check the synthesized Caβ''-alumina pellets for their reversibility to Ca ions in galvanic cells. This cell has been used by Kumar (16) and the present results confirm the fact that the pellets made are solid electrolytes, reversible to calcium at elevated temperatures.

Cells 4.12, 4.13, and 4.14 were set up to establish the activity of CaO in the Caβ''-alumina solid electrolyte. These measurements are necessary in order to characterize the material with the intent of using this electrolyte as an oxygen sensing probe. Although Caβ''-alumina is a Ca ion conducting electrolyte, by fixing the CaO activity in the electrolyte very low oxygen potential electrodes can be measured from a knowledge of these activities. In order to fix the CaO activity, the phase rule predicts an invariant equilibria for a three component, three phase coexistence at constant temperature and pressure. This provides the basis for the three phase compositions which were investigated in cells 4.12 and 4.13.

The measurements carried out on cells 4.2 to 4.14 can also give an indication of the stability of these electrolytes at higher temperatures through extrapolation of the results obtained. This allows one to predict the upper temperature limit for the useful operation of the electrolyte.

The analysis of the EMF data for cells 4.12 and 4.13 is given below and the results are summarized in Figure 6.3. The cell reactions are as follows:

The cathode reaction is:

$$NiO + Ca^{2+} + 2e^- = CaO(\beta'') + Ni \qquad (6.11)$$

The anode reaction is:

$$Ni + CaF_2 = Ca^{2+} + NiF_2 + 2e^- \qquad (6.12)$$

giving the virtual cell reaction:

$$CaF_2 + NiO = NiF_2 + CaO(\beta'') \qquad (6.13)$$

Coexisting Phases	Coexisting Phases
(1) $Ca\beta'' - \alpha Al_2O_3 - MgOAl_2O_3$ – Kumar (16)	(4) $Na\beta Al_2O_3 - \alpha Al_2O_3$ – Elrefaie (10)
(2) $Ca\beta'' - \alpha Al_2O_3 - MgOAl_2O_3$ – This Study	(5) $Na\beta Al_2O_3 - \alpha Al_2O_3$ – Kumar (16)
(3) $Ca\beta'' - MgOAl_2O_3 - 2CaOAl_2O_3$ – This Study	(6) $Na\beta Al_2O_3 - Na\beta'' Al_2O_3$ – Elrefaie (10)
(7) $Ca\beta'' Al_2O_3 - Ca\beta Al_2O_3$ – This Study	

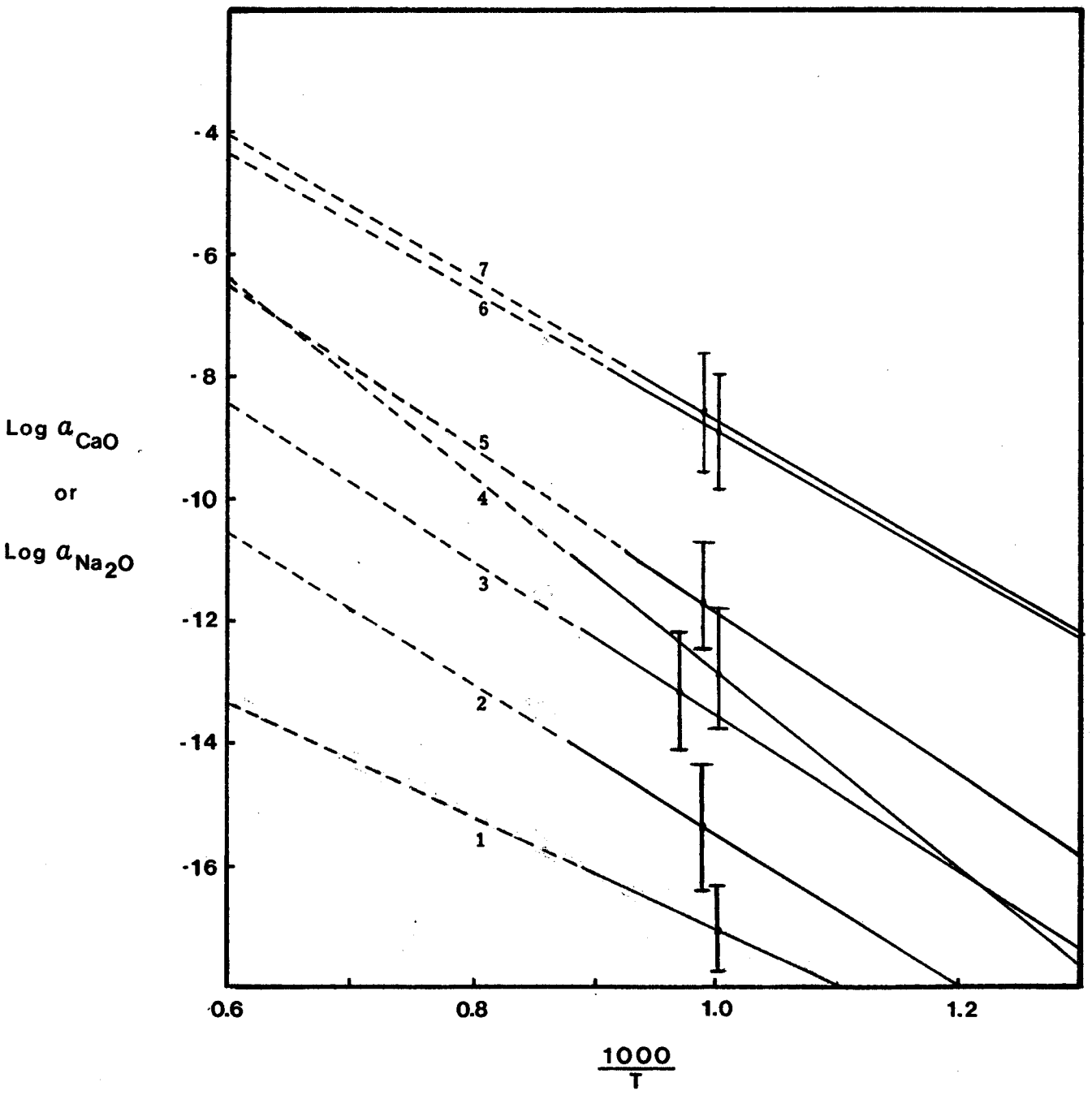

Figure 6.2: Stabilities of some Caβ''-alumina and Naβ-alumina compositions.

From the free energy change of the above reaction and the EMF data we can solve for the activity of CaO(β'') as follows:

$$RT\,\ell n\,aCaO(\beta'') = -nFE + \Delta G^0(NiO) + \Delta G^0(CaF_2) - \Delta G^0(NiF_2) - \Delta G^0(CaO) \quad (6.14)$$

The data used for the evaluation of equation 6.14 are given below in table 6.4.

Equation (6.14) for the three phase compositions "b" and "c" investigated yields:

$$\ell n\,aCaO(\beta'',b) = 1.17 - 25169/T - 3.87\log T \quad (6.15)$$

$$T(K) = 900 - 1100$$

$$\ell n\,aCaO(\beta'',c) = 6.51 - 25750/T - 3.87\log T \quad (6.16)$$

$$T(K) = 900 - 1100$$

Cell 4.14 was also designed to measure the activity of CaO in Caβ''-alumina solid electrolyte, but in this case, a single phase material of composition "a" was investigated. A CSZ solid electrolyte was employed in this cell in order that the Caβ''-alumina solid electrolyte did not directly take part in the cell reaction which might have altered its composition. The anodic, cathodic and virtual cell reactions and analysis for the evaluation of the CaO activity in the electrolyte is given below:

The anode reaction:

$$CeO_2 + \frac{3}{2}CaF_2 + 1e^- = CeF_3 + \frac{3}{2}CaO(\beta'') + \frac{1}{2}O^= \quad (6.17)$$

The cathode reaction:

$$\frac{1}{2}O^= = \frac{1}{4}O_2 + 1e^- \quad (6.18)$$

The virtual cell reaction is:

$$CeO_2 + \frac{3}{2}CaF_2 = CeF_3 + \frac{3}{2}CaO(\beta'') + \frac{1}{4}O_2(cath) \quad (6.19)$$

From the free energy data listed in Table 6.4 and the EMFs measured we can solve for aCaO(β'',a) as follows:

$$RT\,\ell n\,aCaO(\beta'', a) = -nFE + \frac{3}{2}\Delta G^0(CaF_2) + \Delta G^0(CeO_2) - \Delta G^0(CeF_3) - \frac{3}{2}\Delta G^0(CaO) - \frac{1}{4}RT\,\ell n\,PO_2(cath) \quad (6.20)$$

Evaluation of the above expression yields:

$$\ell n\,aCaO(\beta'', a) = 7.05 - 26{,}864/T \quad (6.21)$$

$$T(K) = 950 - 1333$$

The data obtained from relationships 6.15, 6.16 and 6.21 are plotted in Figure (6.2) together with the data from Kumar (16) and Elrefaie (10).

There is no direct way of verifying the accuracy of the results of lines 3 and 7 since this is one of the first measurements of this kind on Caβ"-alumina material. We can however compare directly lines 4 and 5 which show some difference but still lie within experimental error. For line 4 Figure 6.2 Elrefaie (10) used the cell:

$$Pt\,|\,W_{(s)}, WS_{2(s)}\,Na_2S_{(s)}\,|\,Na\ \beta\text{- and }\alpha\text{-}Al_2O_3\,|\,C\ u_2O_{(s)}, Cu_{(s)}\,|\,Pt \quad (6.22)$$

and for line 5 Figure 6.2 Kumar (16) used the cell

$$Pt\,|\,Ag\,(s),\ Ag_2S(s)\,Na_2S(s), (Na_2O)\ \beta/\alpha\,(s)\,|\,CSZ\,|\,Air\,|\,Pt \quad (6.23)$$

The uncertainty in the standard free energy of formation of Na_2S (± 5 kcal) and WS_2 (± 6 kcal) are the major sources of error for these cells.

There is also considerable difference between lines 1 and 2. For line 1 Kumar (16) used the cell:

$$Pt\,|\,Ag\,(s),\ Ag_2S(s), CaSO_4(s)/(CaO)\ \beta''\,(s)\,|\,CSZ\,|\,Air\,|\,Pt \quad (6.24)$$

and in this study cell 4.12 was used. The two lines just fall within experimental error. The discrepancies in the two results may be partially attributed to the uncertainties in the thermodynamic data for CaF_2 (± 5 kcal) and NiF_2 (± 6 kcal). There is also some inconsistency

with the sign in Kumar's data (Ref. 16, Equation 6.13) which has not been resolved in discussion with Kumar.

In general, however, the trend of increasing activity of lime and soda with increases in their concentration, corresponds well to what one would expect to observe. It is clear however that further work is required in this area to resolve the differences observed in the data presented in Figure 6.2.

Table 6.4: Thermodynamic Data Used for Cells 4.12, 4.13 and 4.14

Standard Gibbs Free Energies of Formation		
Compound (ref)	$\Delta G^0(K)$ (calories)	STD Error (± kcal)
NiO (42)	$-56010 + 20.37T$	±2
NiF_2 (35)	$-153500 + 34.2T$	±6
CaO (42)	$-151325 + 23.66T$	±3
CaF_2 (35)	$-293300 - 7.7T\log T + 64.4T$	±5
CeF_3 (35)	$-423234 + 60.0T$	±4
CeO_2 (35)	$-259500 + 47.6T$	±3

Values in calories may be converted to joules by multiplying by 4.182.

CHAPTER 7

DISCUSSION AND CONCLUSIONS

7.1 Periodicity in the Lanthanide Series of Rare Earth Compounds

Seven of the fourteen lanthanide rare earth thiofluoride compounds were investigated in this work. It is possible to estimate the data for the remaining six compounds from a periodic trend one expects to find when going from left to right along a row on the periodic table.

Work carried out by Smoes et al. (31) in measuring the dissociation energies of the lanthanide series of mono-sulphides revealed a characteristic periodicity which agrees with the mono-oxide values measured by other investigators (32). The results of these investigations reveal that the lanthanide series of rare earths exhibit a double periodicity which is the same periodicity observed for the heats of sublimation of the lanthanide metals (33). They concluded from their results as well as from data for the mono-selinides and mono-tellurides that a similar periodicity may pertain to many compounds of the lanthanide series of elements.

The results of Smoes et al.'s investigation of the rare earth mono-sulphides (31) together with the results of Hong (34), on the rare earth oxyfluorides and published data taken from Barin and Knacke (35), on the rare earth sesquioxides are summarized in Figure (7.1). The plotted points for the four compounds exhibit the same general trend. The double periodicity can be clearly seen in this data with the first period extending from gadolinium to ytterbium. The two periods are marked by a sharp discontinuity at europium-gadolinium. Since a good correlation is observed between the various data sets [see

Figure (7.1)], estimates of the free energies of formation of the six remaining thiofluoride compounds can be obtained.

7.2 Desulphurization Capacity of the ReOF Compounds

From the thermodynamic data for reaction (6.8) which is plotted in Figure (6.2), we see that of the rare earth compounds investigated, lanthanum and cerium (which are the two most abundant constituents found in bastnaesite concentrates) show the greatest potential for desulphurization.

The LaOF-LaSF equilibria is plotted on the La-S-O phase stability diagram reproduced from Kumar (16) in Figures (7.2) and (7.3). These plots predict that for both desulphurization of gas mixtures and liquid steel, for a given oxygen potential, the desulphurization ability of La_2O_3 is much better than that of LaOF. The desulphurization ability of LaOF increases with decreasing oxygen potential. It can be seen from Figure (7.3), that in order to achieve effective desulphurization using LaOF, very low oxygen potentials as obtained in Ca and Mg treatments are required. Since Ca and Mg are strong desulphurizers as well, LaOF is not a viable alternative for desulphurization of liquid steel.

We can conclude from these results, that in processes using bastnaesite for gaseous desulphurization, the CeO_2 present in the concentrate is largely responsible for desulphurization and that the ReOF compounds are essentially inactive in the desulphurization reactions taking place.

7.3 The Chemical Stability of Caβ″-Alumina in Contact with Low Oxygen Potentials

The feasibility of using Caβ-alumina solid electrolytes as sensors in the low oxygen partial pressure and high temperature environments which are encountered in liquid steel

Figure 7.1:

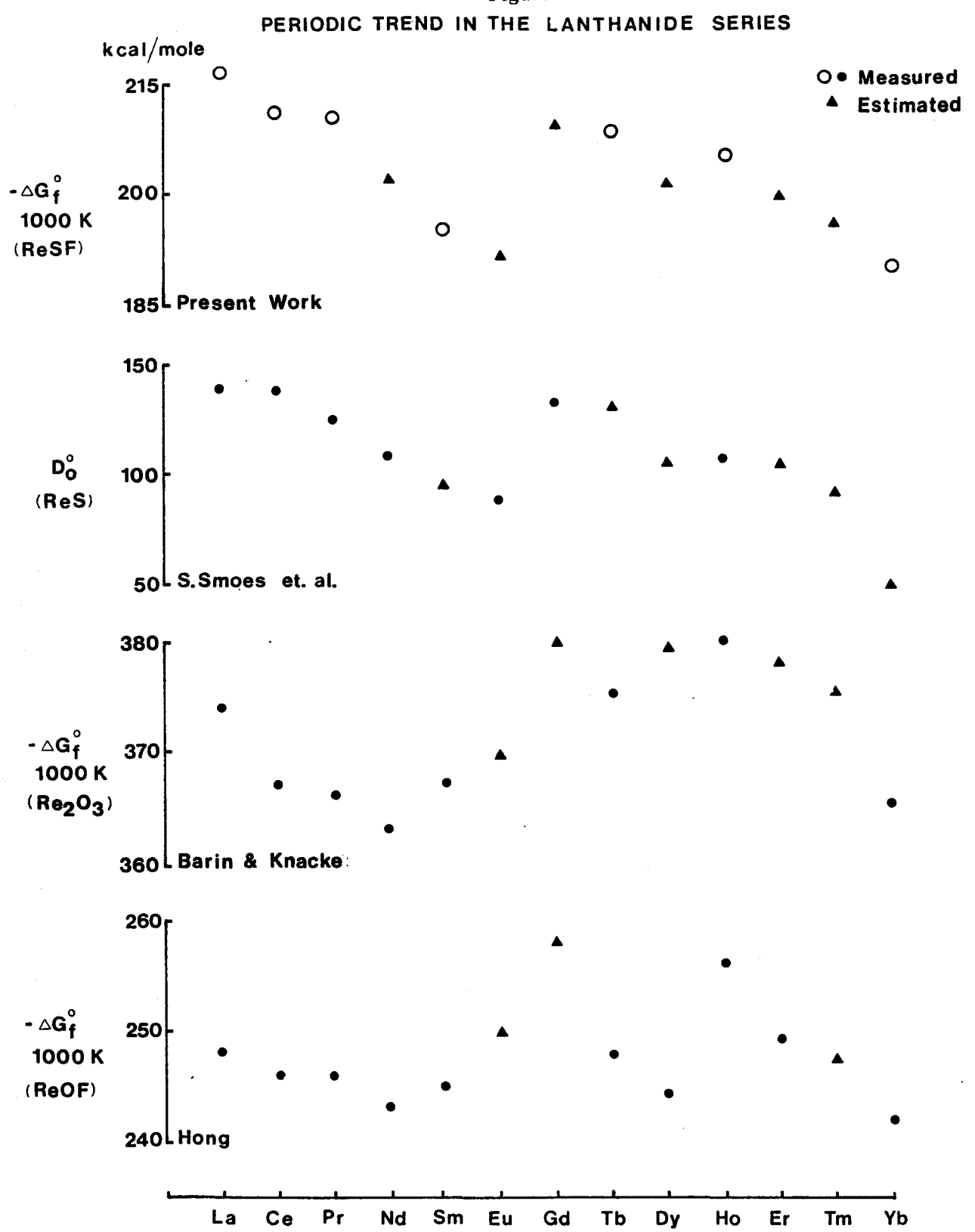
PERIODIC TREND IN THE LANTHANIDE SERIES
kcal/mole
Measured
Estimated
$-\Delta G_f^\circ$ 1000 K (ReSF)
215
200
185
Present Work
150
D_o° (ReS)
100
50
S.Smoes et. al.
380
$-\Delta G_f^\circ$ 1000 K (Re_2O_3)
370
360
Barin & Knacke
260
$-\Delta G_f^\circ$ 1000 K (ReOF)
250
240
Hong
La
Ce
Pr
Nd
Sm
Eu
Gd
Tb
Dy
Ho
Er
Tm
Yb

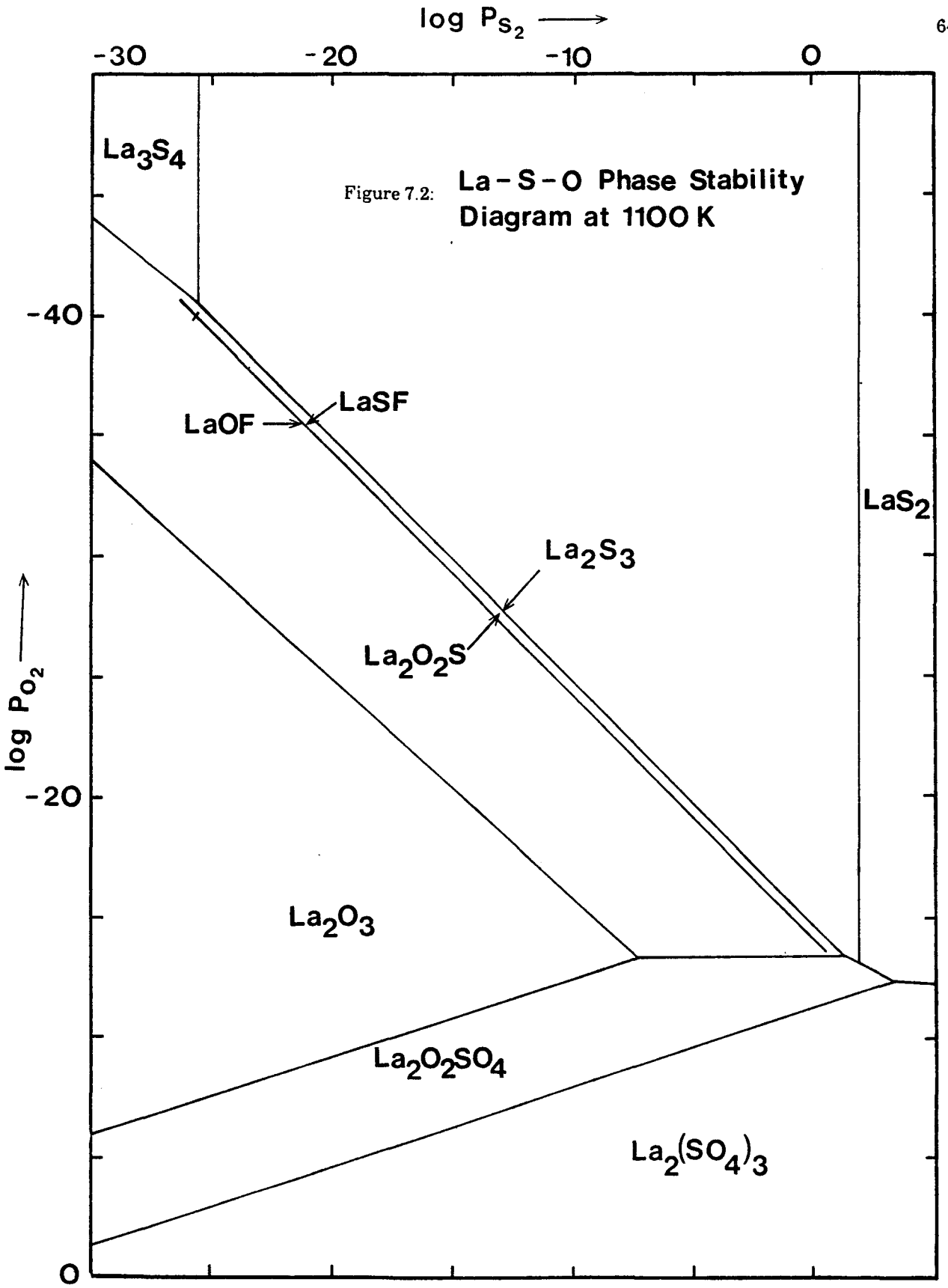

Figure 7.2: La-S-O Phase Stability Diagram at 1100 K

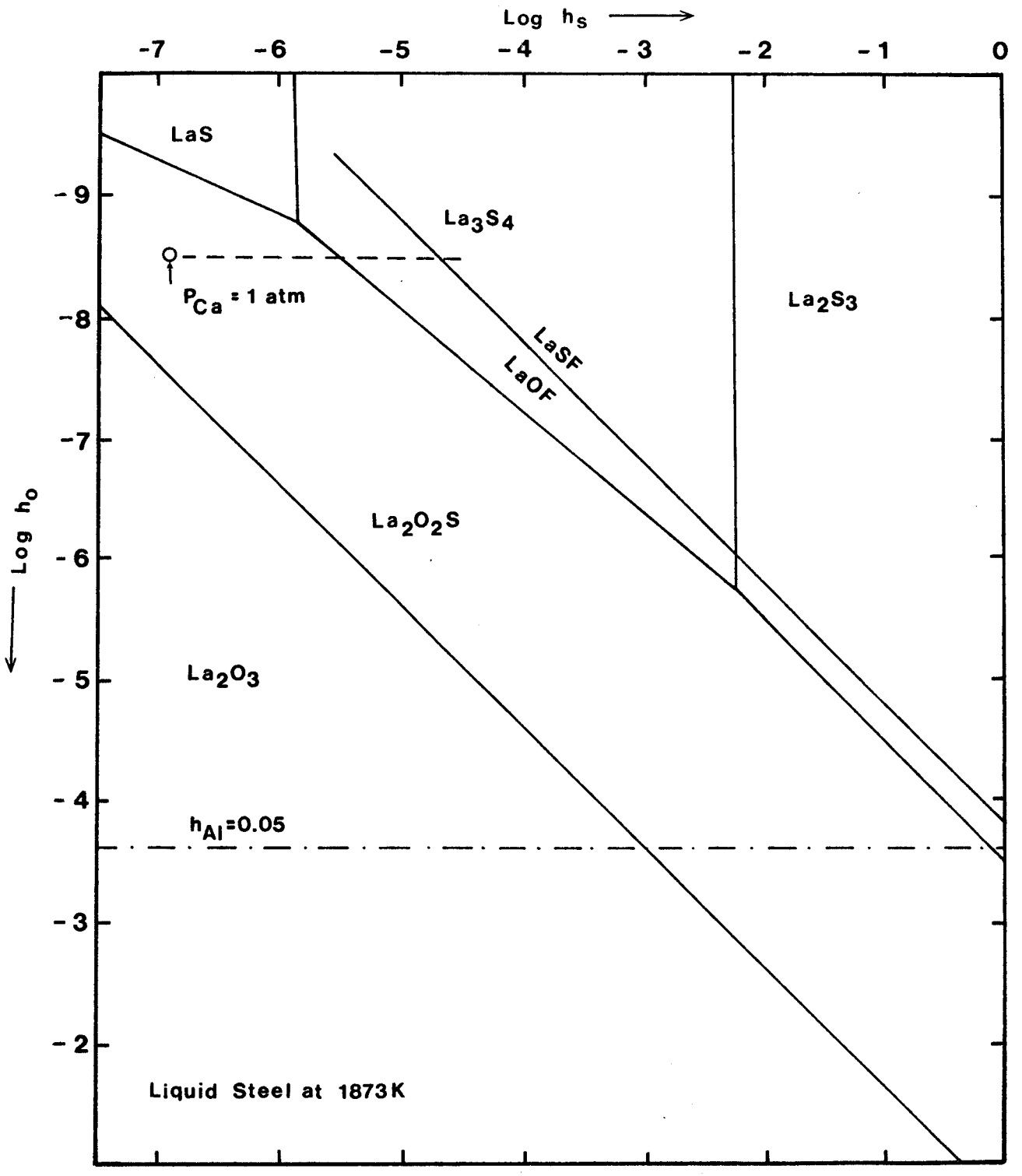

Figure 7.3: La-S-O phase stability diagram in terms of Henrian activities at 1873K.

and iron is established in this section. It is essential to establish the chemical stabilities of the Caβ-aluminas in the environments in which they are proposed to be used. In order to determine the effects of temperature and low oxygen partial pressures on the stabilities of the Caβ-aluminas the following reactions are considered:

$$CaO(a), (b), (c) = Ca(g) + \frac{1}{2}O_2(g) \tag{7.1}$$

$$\Delta G°(7.1) = -RT\,\ell n\,(P(Ca)\,PO_2^{1/2}/a_{CaO}) \tag{7.2}$$

Combining the above two equations and solving for $\ell n\, P(Ca)$ we obtain the following relation:

$$\ell n\, P(Ca) = -1/2\, 1n\, PO_2 + 1n\, a_{CaO} - \Delta G^0(7.1)/RT \tag{7.3}$$

Equation (3) can be solved for each Caβ-alumina composition investigated by combining equations 6.15, 6.16 and 6.21 derived earlier with equations 7.3. In order to evaluate the effects of low oxygen potentials on these solid electrolyte materials the oxygen potential in equation 7.3 is that established by the Al/Al_2O_3 equilibria and the results obtained are:

$$1n\, P[Ca(a)] = -54467/T + 0.629 \log T + 15.04 \tag{7.4}$$

$$T = 950 - 1333K$$

$$1n\, P[Ca(b)] = -52772/T - 3.24 \log T + 9.16 \tag{7.5}$$

$$T = 900 - 1100K$$

$$1n\, P[Ca(c)] = -55353/T - 3.24 \log T + 14.5 \tag{7.6}$$

$$T = 900 - 1100\,K$$

The above relationships are extrapolated to higher temperatures and plotted in Figure (7.4). The calcium partial pressures are lowest for composition (b) indicating that this composition is the most stable of the three. From Figure (7.4) it is evident however, that all compositions are chemically stable under these oxygen partial pressures and temperatures up

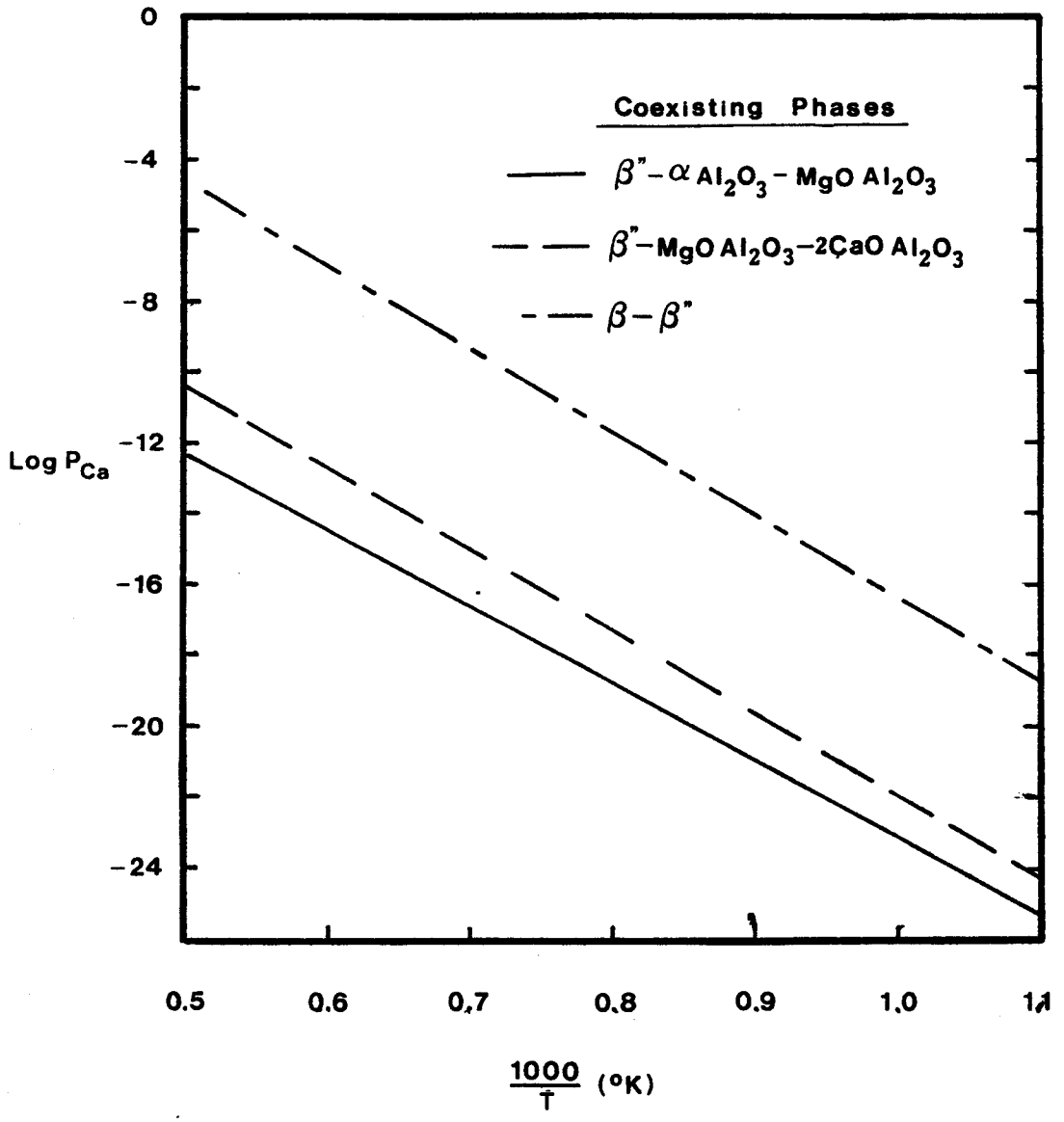

Figure 7.4: Variation of P_{Ca} with temperature, in contact with an oxygen partial pressure corresponding to the Al/Al_2O_3 coexistence.

to 2000K. We can conclude that these solid electrolyte materials are suitable for use as calcium and oxygen sensors in environments such as liquid iron and steel provided suitable cells can be designed.

REFERENCES

1. Meng, V.V.M., "High Temperature Gaseous Desulphurization Using Cerium Oxides and Bastnaesite Concentrates", Ph.D. Thesis, McMaster University (1985).

2. Zachariasen, W.H., Acta Cryst., V4, 231 (1951).

3. Finkelnberg, W., and Stein, A., Journ. Chem. Phys., V18, 1296 (1950).

4. Baenziger, N.C. et al., Acta Cryst., V76, 4734-4735 (1954).

5. Hong, Y.R., Kumar, R.V., Kay, D.A.R., Proceedings of the International Conf., on Rare Earth Develop. and Applications, VII, 1194-1203 (1985).

6. Hong, Y.R., Kay, D.A.R., Unpublished Work.

7. Schmid, R. and Hahn, H., Seitshrift Für Anorg., und Allgem. Chem., V373, 168-175 (1985).

8. Verkhovets, M.N., Kamarzin, A.A., Sokolov, U.V., I. Sv. OTD Akad. Nauk. SSSK Ser Khim Nauk. Nos. 4-6, 125-126 (1973).

9. Choudhury, J., Electrochem. Soc., V120, 1663 (1973).

10. Elrefaie, F. Ph.D. Thesis, McMaster University (1982).

11. Yao, Y.F.Y., Kummer, J.T., J. Inorg. Nucl. Chem., V29, 2453 (1967).

12. Radzilowoski, R.H. Inorg. Chem., V8, 994 (1969).

13. Radzilowoski, R.H., Kummer, J.T., Inorg. Chem., V8, 2531 (1969).

14. Whittingham, M.S., Helliwell, R.W., Higgins, R.A., U.S. Gov't Res. Dev. Report, V69, 228 (1969).

15. Saalfield, H., Matthies, H., S.K. Datta Ber. Deut. Keram. Ges., V45, 212 (1968).

16. Kumar, R.V., "Use of Calcia Stabilized Zirconia and β-β" Alumina Solid Electrolytes in Galvanic Cells", Ph.D. Thesis, McMaster University (1984).

17. Kiukkola, K., Wagner, C., J. Electrochem. Soc., V104, 308 (1957).

18. Rapp, R.A., "Physicochemical Measurements in Metal Research", Part 2, Wiley-Interscience, New York (1978).

19. Farrington, G.C. and Dunn, B., Solid State Ionics, V7, 267 (1982).

20. Devries, R.C. and Roth, W.L., J. Amer. Cer. Cos., V52, 364 (1969).

21. Weber, N., and Venero, A.F., 72nd Annual Meeting of the American Cer. Soc., May 1970, Paper 5-J1-70.

22. Beevers, C.A. and Ross, M.A., Z. Krist., V97, 59 (1937).

23. Kummer, J.T., Solid State Chem., V7, 141 (1972).

24. Schmalzried, Proc. Int. Symp. Met. Chem., London, MNSO (1972).

25. Patterson, J.W., et al., J. Electrochem. Soc., V114, 752 (1967).

26. Steel, B.C.H., and Alcock, C.B., Trans AIME, V233, 1359 (1965).

27. Alcock, C.B. (Editor) "Electromotive Force Measurements in High Temp Systems", American Elsevier Pub. Co. Inc. (1968).

28. Mills, K.C., "Thermodynamic Data for Inorganic Sulfides, Selenides and Telurides", Butterworths, London (1974).

29. Kumar, R.V. and Kay, D.A.R., Met. Trans. B., V16B, 107-112 (1985).

30. Choudhury, N.S., "Solid Electrolytics", Topics in Applied Physics, Springer-Verlag, (1977).

31. Smoes, S., et al., Trans. of the Faraday Soc., V65, 682-687 (1969).

32. Ames, L.L. et al., J. Physic Chem., V71, 2707, (1967).

33. Habermann, C.E., Daane, A.H., J. Chem. Physics, V41, 2818 (1964).

34. Hong, Y.H., Kay, D.A.R., Unpublished Data, McMaster University.

35. Barin, I., Knacke, O., Kubaschewski, O., "Thermochemical Properties of Inorganic Substances", Vol. 1 and Vol. 2, Supplement (1977).

36. Hagoptan, C., "Desulfuriztion Using Rare Earth Oxides", B.Sc. Thesis, McMaster University (1978).

37. Rapp, R.A., "Physicochemical Measurements in Metal Research", Part 2, Wiley Interscience, New York (1978).

38. Geller, S. (Editor) "Solid Electrolytes", Topic in Applied Physics, Springer-Verlag (1977).

39. Subbarao, E.C., "Solid Electrolytes and their Applications", Plenum Press, New York (1980).

40. Carter, R.E., Roth, W.L., "Electromagnetic Force Measurements on High Temperature Systems", ed. C.B. Alcock, Institute of Mining and Metals, London, 125, (1960).

41. Goto, K., Pluschkell, N., "Physics of Electrolytes", ed. J. Hladtk, V2, Academic Press, 540 (1972).

42. Kubaschewski, O., Alcock, C.B., "Metallurgical Thermochemistry", 5th Edition, International Series on Materials Science and Technology, ed. G.V. Raynor, (1977).

43. Janaf Thermochemical Tables, Second Edition (1971).

44. Gshneidner, K.A., Kippenham, N., McMasters, O.D., "Thermochemistry of the Rare Earths", Report No. IS-RIC-6, Rare Earth Information Centre, Institute for Atomic Research, Iowa University, Iowa (1973).

45. Gshneidner, K.A., Kippenham, N., Report No. IS-RIC-5 Rare Earth Information Centre, Institute for Atomic Research, Iowa University, Iowa (1973).

46. F.A. Bannister, M.H. Hey, Min. Mag., 23, 587 (1934).

APPENDIX I

Table A1: Elemental Analysis of Bastnaesite Concentrates –% by weight*

Component	Concentrate				Error	Present in Ore as uncalcined/calcined
	Uncalcined		calcined			
	4000	4010	4000C	4100		
Ce	28.10	32.30	31.00	38.70	±1.0	$RE(OH)_{1-x}F_xCO_3/CeO_2$
La	16.30	18.70	18.00	23.80	±0.5	$RE(OH)_{1-x}F_xCO_3$/REOF
Nd	6.30	7.30	7.10	8.10		$RE(OH)_{1-x}F_xCO_3$/REOF
Pr	2.30	2.65	2.55	3.00		$RE(OH)_{1-x}F_xCO_3$/REOF
Sm	0.30	0.35	0.34	0.38		$RE(OH)_{1-x}F_xCO_3$/REOF
Gd	0.14	0.16	0.14	0.19		$RE(OH)_{1-x}F_xCO_3$/REOF
Other	0.05	0.056	0.054	0.060		$RE(OH)_{1-x}F_xCO_3$/REOF
Total RE	53.49	61.52	59.18	74.23		
F	4.15	4.60	4.10	5.00	±0.25	$RE(OH)_{1-x}F_xCO_3$/REOF
CO_2	19.51	20.70	8.48	4.05		$RE(OH)_{1-x}$ F_xCO_3 $CaCO_3$ $CaCO_3$ and residual RE carbonates
Sr	5.70	1.10	7.10	1.20		strontianite
Ca	4.25	0.71	6.70	0.64		calcite
Ba	1.12	0.78	1.03	1.20		barite
Fe	0.43	0.39	0.47	0.39		
AL	0.10	0.08	0.11	0.08		
Mg	0.29	0.17	0.33	0.18		acmite
Na	0.022	0.016	0.025	0.023		
K	0.025	0.027	0.030	0.018		
P	0.46	0.34	0.43	0.56		
Balance (mainly oxygen)	10.45	9.57	12.02	12.43		

* V. Meng (1)

Table A2: Compositional Analysis of Bastnaesite Concentrates*

Element	Moles of Element in 100 g				Error
	4000	4010	4000C	4100	
Ce	0.2005	0.2305	0.2212	0.2762	±0.006
La	0.1173	0.1346	0.1296	0.1713	±0.004
Total RE	0.3811	0.4382	0.4216	0.4729	
F	0.2184	0.2421	0.2158	0.2632	±0.013
CO_2	0.4434	0.4705	0.1927	0.0921	
Ca	0.1060	0.0177	0.1672	0.0160	
	Molar Ratios				
F/RE(1)	0.573	0.552	0.512	0.556	
CO_2/(RE + Ca)(2)	0.91	1.03	N/A	N/A	
CO_2/Ca(3)	N/A	N/A	1.15	5.76	
F/(RE–Ce)(4)	1.21	1.17	1.08	1.34	

(1) This gives the value of x in $RE(OH)_{1-x} F_x CO_3$

(2) The carbonate content of uncalcined concentrates is present as $RE(OH)_{1-x} F_x CO_3$ and $CaCO_3$. A theoretical value of 1 should be obtained.

(3) In calcined concentrates the carbonates are mainly present as calcite (since process temperatures used by manufacturer are too low to decompose this mineral). A theoretical value of 1 should be obtained. Larger values indicate the presence of residual rare earth carbonates.

(4) This ratio would be equal to 1.0 if the fluorine was associated with rare earth elements other than cerium. A value greater than one suggests that at least part of the cerium is associated with the fluoride.

* V. Meng (1)

APPENDIX II

The powder diffraction patterns for the rare earth thiofluorides found in this investigation are listed on the following pages.

The diffraction patterns for LaSF and CeSF were determined by R. Schmid and H. Hahn (7) and the patterns found in this investigation agree with those obtained by the aforementioned authors, and can be found in the above reference.

POWDER DIFFRACTION PATTERNS

Cu-Kα SOURCE

YSF			PrSF		
2θ	d-SPACING	I/IO	2θ	d-SPACING	I/IO
26.31	3.384	50.2	26.01	3.423	100
26.77	3.327	30.3	32.11	2.785	51.1
27.20	3.276	92.9	41.58	2.170	60.3
33.86	2.645	70.7	41.78	2.16	17.9
35.7	2.511	48.5	45.59	1.988	42.9
43.34	2.086	100.0	53.54	1.710	45.1
46.96	1.933	67.3	53.60	1.708	25.5
48.49	1.876	52.5	66.63	1.402	28.3
55.93	1.643	26.9	66.81	1.399	27.7
56.47	1.628	35.0	81.87	1.175	18.5
69.6	1.349	34.3			
86.69	1.122	25.9			
93.49	1.057	20.2			

POWDER DIFFRACTION PATTERNS

Cu-Kα SOURCE

SmSF			HoSF		
2θ	d-SPACING	I/IO	2θ	d-SPACING	I/IO
20.03	4.429	16.3	23.96	3.711	16.9
25.83	3.446	48.8	26.47	3.364	51.2
26.37	3.337	100.0	27.35	3.258	100.0
26.5	3.361	40.7	33.96	2.637	72.0
32.66	2.740	69.8	34.17	2.622	22.7
32.81	2.727	30.2	35.83	2.504	32.9
34.86	2.57	32.6	45.60	1.987	18.8
42.16	2.13	26.7	47.20	1.931	44.4
45.99	1.972	59.3	47.25	1.922	22.7
46.10	1.967	40.7	48.66	1.869	37.2
46.87	1.937	44.2	56.15	1.637	20.8
54.43	1.684	36.0	56.59	1.625	30.9
54.6	1.679	50.0	69.84	1.384	24.6
67.71	1.383	30.2			

POWDER DIFFRACTION PATTERN

Cu-Kα SOURCE

TbSF			YbSF		
2θ	d-SPACING	I/IO	2θ	d-SPACING	I/IO
26.04	3.419	38.9	21.58	4.11	100.0
26.16	3.403	2.18	26.28	3.388	68.3
26.75	3.329	100.0	26.39	3.374	40.4
27.01	3.298	26.4	44.07	2.053	31.7
33.26	2.691	65.3	45.34	1.998	76.0
35.27	2.542	25.5	45.55	1.989	34.6
42.75	2.113	79.6	50.85	1.794	57.7
46.41	1.955	47.2	50.97	1.790	37.5
47.74	1.904	42.1	65.18	1.43	28.8
55.26	1.661	32.4			
55.57	1.652	36.1			
68.84	1.363	38.0			
85.53	1.344	23.6			

APPENDIX III

EMF* DATA FOR CELLS 4.1 TO 4.14

Cell 4.1 - 4 cells

(A)

Temp (K)	EMF (V)
919	1.058
984	1.045
1012	1.040
1063	1.030

(B)

Temp (K)	EMF (V)
935	1.055
999	1.042
1028	1.037
1055	1.031

(C)

Temp (K)	EMF (V)
944	1.053
990	1.044
1034	1.036
1076	1.027

(D)

Temp (K)	EMF (V)
923	1.057
978	1.047
1036	1.034
1088	1.025

Cell 4.2 - 2 cells

(A)

Temp (K)	EMF (V)
953	1.060
1003	1.053
1042	1.047
1073	1.043

(B)

Temp (K)	EMF (V)
925	1.064
993	1.054
1047	1.047
1086	1.041

* Error associated with these measured is $\pm .001$ V.

Cell 4.3 - 2 cells

(A)		(B)	
Temp (K)	EMF (V)	Temp (K)	EMF (V)
931	1.102	953	1.099
984	1.095	991	1.094
1029	1.088	1036	1.087
1078	1.081	1083	1.080

Cell 4.4 - 2 cells

(A)		(B)	
Temp (K)	EMF (V)	Temp (K)	EMF (V)
935	1.136	923	1.139
975	1.129	1001	1.124
1021	1.121	1037	1.117
1084	1.107	1074	1.110

Cell 4.5 - 2 cells

(A)		(B)	
Temp (K)	EMF (V)	Temp (K)	EMF (V)
961	1.210	933	1.219
1008	1.195	979	1.204
1065	1.177	1046	1.183
1085	1.171	1072	1.175

Cell 4.6 - 2 cells

(A)		(B)	
Temp (K)	EMF (V)	Temp (K)	EMF (V)
948	1.184	939	1.186
980	1.170	967	1.175
1026	1.151	1030	1.150
1073	1.133	1087	1.127

Cell 4.7 - 2 cells

(A)		(B)	
Temp (K)	EMF (V)	Temp (K)	EMF (V)
913	1.252	920	1.251
989	1.243	984	1.243
1037	1.237	1029	1.238
1090	1.230	1075	1.232

Cell 4.8 - 3 cells

(A)		(B)		(C)	
Temp (K)	EMF (V)	Temp (K)	EMF (V)	Temp (K)	EMF (V)
928	1286	935	1284	925	1286
976	1277	980	1276	987	1275
1037	1266	1024	1268	1032	1267
1069	1261	1073	1260	1087	1257

Cell 4.9 - 1 cell

Temp (K)	EMF (V)
894	0.245
967	0.250
1031	0.253
1058	0.255

Cell 4.10 - 1 cell

Temp (K)	EMF (V)
888	0.243
949	0.248
998	0.251
1047	0.256

Cell 4.11 - 1 cells

Temp (K)	EMF (V)
876	0.243
946	0.247
1002	0.250
1076	0.256

Cell 4.12 - 2 cells

(A)

Temp (K)	EMF (V)
890	0.593
946	0.625
987	0.646
1054	0.680

(B)

Temp (K)	EMF (V)
872	0.585
918	0.608
1006	0.656
1079	0.695

Cell 4.13 - 2 cells

(A)		(B)	
Temp (K)	EMF (V)	Temp (K)	EMF (V)
905	0.418	882	0.413
933	0.427	901	0.417
990	0.445	974	0.440
1048	0.463	1069	0.468

Cell 4.14 - 1 cell

Temp (K)	EMF (V)
1050	1.061
1113	1.027
1203	0.982
1333	0.915